

HIGH VOLUME FLY ASH CONCRETES FOR SUSTAINABLE APPLICATIONS
IN CONSTRUCTION

by

Elifsu Balcı

B.S., Civil Engineering, Boğaziçi University, 2018

Submitted to the Institute for Graduate Studies in
Science and Engineering in partial fulfillment of
the requirements for the degree of
Master of Science

Graduate Program in Civil Engineering
Boğaziçi University

2022

ACKNOWLEDGEMENTS

First of all, I would like to express my sincere gratitude to my advisor Prof. Nilüfer Özyurt Zihnioğlu, and my co-advisor Prof. Turan Özturan for their consistence support and guidance during my thesis study.

I also would like to thank construction material laboratory assistants Onur Öztürk, Olcay Gurabi Aydoğan and former assistants Assis. Prof. Hasan Yıldırım, Assis. Prof. Ahmet Onur Pehlivan, Assoc. Prof. Anıl Niş and Assis. Prof. Abdullah Huzeyfe Akça for sharing their valuable experiences with me.

I am grateful to Ümit Melep for his technical assistance during to experimental studies that were conducted.

I am also thankful to my colleagues Alphan Ali Dilber, Arda Sepetci, Aydın Ata, and Ece Bihter Dal for their support.

I also would like to thank Akçansa and Boğaziçi Beton for supplying the necessary materials during the experiments.

Finally, I am extremely grateful to my mother Meral Balcı, my father Yücel Balcı, and my sister Işıl Balcı for their endless support.

ABSTRACT

HIGH VOLUME FLY ASH CONCRETES FOR SUSTAINABLE APPLICATIONS IN CONSTRUCTION

Reducing CO₂ emission has become one of the most important subjects that the world focuses. Various actions are taken to make the construction materials and methods sustainable since the construction industry has a great contribution to the world's CO₂ emissions. Replacement of cement with alternative binders is considered the most efficient and practical way to increase the sustainability of concrete. Fly ash usage in concrete has several effects for increasing sustainability. It decreases the use of cement and environmental pollution while it enhances some properties of concrete. Increased level of replacement further decreases environmental damage made by the production of concrete if targeted performance parameters could be obtained. In this study, the fresh properties, strength properties, and durability properties of different concrete mixtures were examined. The structural design of an industrial floor was made by using these ordinary concrete (PCC) and high-volume fly ash concrete (HVFAC), and the materials were compared by means of required thickness, environmental impact, and economic impact. Two replacement levels (40-60%) and two water/binder ratios (W/B) (0.35-0.50) were considered, and the mechanical properties of the mixtures were determined. Based on TR34, thickness design for an industrial floor was done for all concrete series. Environmental and economic impact analysis was done for all concrete series. Compared to PCC mixtures, lower mechanical properties, higher thickness requirements, and lower environmental impact values were found for HVFAC mixtures. With decreasing W/B, enhanced performance parameters were obtained for both PCC and HVFAC mixtures. The results of this study show that the environmental impact of concrete could be further decreased by increasing the replacement level of fly ash and still targeted performance parameters could be obtained from industrial floors.

ÖZET

SÜRDÜRÜLEBİLİR İNŞAAT UYGULAMALARI İÇİN YÜKSEK HACİMDE UÇUCU KÜLLÜ BETONLAR

Artan nüfus, enerji ve doğal kaynakların harcanma hızı ve CO₂ salınımları hiç olmadığı kadar arttırdı. İnşaat sektörünün CO₂ salınımindaki payının büyük olması, insanlığı bu sektörde kullanılan malzeme ve metotları daha çevreci hale getirmeye yöneltti. Betonun CO₂ salınımını azaltmak için içerisindeki çimentonun belli bir miktarı yerine farklı bağlayıcı malzemeler kullanılması, en etkili ve uygulanabilir yöntemlerden biri olarak görülüyor. Çimento yerine uçucu kül kullanılması betonu birçok yönden daha çevreci hale getiriyor: çimento miktarının azaltılması, endüstriyel atığının hammadde olarak kullanılmasıyla çevresel kirliliğin azaltılması ve beton özelliklerinin geliştirilmesi. Tasarımda ihtiyaç duyulan özellikler sağlandığı sürece betondaki uçucu kül oranının artışı betonu daha çevreci ve sürdürülebilir bir ürün haline getirecektir. Bu çalışmada farklı beton karışımları için taze hal, dayanım ve dayanıklılık özellikleri test edildi. Özellikleri belirlenen bu standart beton ve yüksek uçucu küllü betonlar için, endüstriyel zemin tasarımı yapılarak ihtiyaç duyulan zemin kalınlığı ve bu zeminlerin çevresel etkileri karşılaştırıldı. %40 ve %60 olmak üzere iki farklı uçucu kül/bağlayıcı oranı ve 0.35 ve 0.50 olmak üzere iki farklı su/bağlayıcı oranı çalışıldı. Bu karışımların mekanik özellikleri hesaplanıp, TR34'e uygun şekilde endüstriyel zemin tasarımları yapıldı. Tasarlanan bu zeminler için ihtiyaç duyulan malzeme miktarları dikkate alınarak, bu karışımlar ekonomik ve çevresel açıdan incelendi. Bu çalışma gösteriyor ki, yüksek uçucu küllü betonlar, standart betonlara göre daha düşük mekanik özellikler gösterip aynı yüke maruz kalan endüstriyel zeminde daha fazla kalınlık ihtiyacı yaratsa da çevresel etkisi ve maliyeti daha düşük kalıyor. Bu çalışmanın sonucunda çimentonun uçucu kül ile yüksek oranlarda değiştirilmesi ile aynı yük durumuna hizmet edecek daha çevreci ve ekonomik beton tasarlanmanın mümkün olduğu gösteriliyor.

TABLE OF CONTENTS

ACKNOWLEDGEMENTS	iii
ABSTRACT	iv
ÖZET	v
LIST OF FIGURES	ix
LIST OF TABLES	xii
LIST OF SYMBOLS	xiv
LIST OF ACRONYMS/ABBREVIATIONS	xv
1. INTRODUCTION	1
1.1. What is the Origin of Fly Ash?	3
1.2. Classification of Fly Ash	5
1.2.1. Early Classification According to SiO_2 , Al_2O_3 , CaO , and SO_3 Content	5
1.2.2. According to CaO Content	6
1.3. Fly Ash Use in Concrete	7
1.3.1. EN 206 Instruction for Fly Ash in Concrete	7
1.3.2. Literature Review	8
1.3.2.1. Fresh State Properties	8
1.3.2.2. Strength Properties	9
1.3.2.3. Durability Properties	12
1.3.2.4. Analysis	13
2. MATERIALS AND METHODS	14
2.1. Materials	14
2.1.1. Cement	14
2.1.2. Fly Ash	15
2.1.3. Aggregates	16
2.1.4. Chemical Admixture	18
2.2. Mixture Design	18
2.2.1. Specimen Curing	19

2.3. Experimental and Calculating Methods	20
2.3.1. Fresh State Tests	20
2.3.1.1. Slump Test	20
2.3.1.2. Fresh State Density Test	20
2.3.2. Strength Tests	21
2.3.2.1. Compressive Strength Test	21
2.3.2.2. Three-Point Bending Test	21
2.3.2.3. Fracture Parameter Calculation	22
2.3.3. Durability Tests	25
2.3.3.1. Resonance Frequency Test	25
2.3.3.2. Water Absorption Test	26
2.3.3.3. Sorptivity Test	27
2.3.3.4. Length Change Test	29
2.3.3.5. Abrasion Test	29
2.3.3.6. Freeze-Thaw Test	30
2.3.4. Design and Analysis	31
2.3.4.1. Thickness Design of Industrial Floor	31
2.3.4.2. Environmental Analysis of the Industrial Floor	33
2.3.4.3. Economic Analysis of the Industrial Floor	34
3. RESULTS AND DISCUSSION	35
3.1. Fresh State Test Results	35
3.1.1. Slump Test Results	35
3.1.2. Fresh Density Test Results	35
3.2. Strength Test Results	36
3.2.1. Compressive Strength Test Results	36
3.2.2. Three-Point Bending Test Results	38
3.2.3. Fracture Analysis from Three Point Bending Test	39
3.3. Durability Test Results	42
3.3.1. Resonance Frequency Test	42
3.3.2. Water Absorption Test Results	45
3.3.3. Sorptivity Test	47

3.3.4. Length Change Test	50
3.3.5. Abrasion Test	51
3.3.6. Freeze-Thaw Test	52
3.4. Design and Analysis	54
3.4.1. Thickness Design of an Industrial Floor	54
3.4.2. Environmental Analysis for 2000 m ² Industrial Floorl	56
3.4.3. Economic Analysis for 2000 m ² Industrial Floor	57
4. CONCLUSION	59
REFERENCES	61
APPENDIX A: COPYRIGHTS OF FIGURES	68

LIST OF FIGURES

Figure 1.1.	Fly ash collection prosses at thermal power plant [9].	4
Figure 2.1.	Gradation curve of the mix of aggregates with respect to reference curves (TS802 [38]).	18
Figure 2.2.	Slump test.	20
Figure 2.3.	Compressive strength test.	21
Figure 2.4.	Three-point bending test.	22
Figure 2.5.	Longitudinal resonance frequency test.	25
Figure 2.6.	Water absorption test stages- (a) oven drying procedure (b) saturation after immersion procedure (c) saturation after boiling procedure (d) immersed apparent mass procedure.	27
Figure 2.7.	Sorptivity test.	28
Figure 2.8.	Length change measurement.	29
Figure 2.9.	Abrasion test.	30
Figure 2.10.	Freeze-thaw test.	31
Figure 3.1.	Compressive strength test results.	37
Figure 3.2.	Flexural strength test results.	38

Figure 3.3.	Initial cracking toughness.	40
Figure 3.4.	Unstable fracture toughness.	40
Figure 3.5.	Relation between flexural strength and initial cracking toughness and unstable fracture toughness.	41
Figure 3.6.	Relationship between compressive strength and dynamic modulus of elasticity calculated from resonance frequency test results. . . .	43
Figure 3.7.	Relationship between the slope of the elastic region of bending test results and dynamic modulus of elasticity calculated from resonance frequency test results at the age of 28 days.	44
Figure 3.8.	Relationship between the slope of the elastic region of bending test results and dynamic modulus of elasticity calculated from resonance frequency test results at the age of 90 days.	44
Figure 3.9.	Relationship between volume of permeable pore space (voids), %, and compressive strength (MPa) for mixtures prepared with 0.5 W/B ratio.	46
Figure 3.10.	Relationship between volume of permeable pore space (voids), %, and compressive strength (MPa) for mixtures prepared with 0.35 W/B ratio.	46
Figure 3.11.	Initial rate of absorptions.	48
Figure 3.12.	Secondary rate of absorptions.	49
Figure 3.13.	Length changes for all six mixtures.	50

Figure 3.14. Relationship between flexural strength and mass loss which represent abrasion level of concrete.	52
Figure 3.15. Relative dynamic modulus of elasticity.	53
Figure 3.16. Flexural tensile strength and thickness relation.	56
Figure 3.17. CO ₂ emissions for 2000 m ² industrial floor with design thickness. .	57
Figure 3.18. Cost for 2000 m ² industrial floor with design thickness.	58
Figure A.1. Copyrights of Figure 1.1.	68

LIST OF TABLES

Table 1.1.	Chemical composition of fly ash according to the coal it is obtained [10].	5
Table 1.2.	Classification of fly ash as Type I, II, III, and IV [11].	6
Table 2.1.	Chemical properties of cement (TS EN 196-2 [30]).	14
Table 2.2.	Physical properties of cement (TS EN 196-3 [31] and TS EN 196-6 [32]).	15
Table 2.3.	Mechanical properties of cement (TS EN 196-1 [33]).	15
Table 2.4.	Chemical properties of fly ash (TS EN 196-2 [30] and ICP-OES). .	16
Table 2.5.	Physical properties of fly ash (TS EN 450-1 [34] and TS EN 451-2 [35]).	16
Table 2.6.	Physical properties of aggregates (EN 1097-6 [36]).	17
Table 2.7.	Sieve analysis results of aggregates (EN 933-1 [37]).	17
Table 2.8.	Mixture notations.	19
Table 2.9.	Mix proportions.	19
Table 2.10.	The constants a_i , b_i , c_i , d_i , e_i , f_i , and calculate M_i values [45]. . . .	25
Table 2.11.	CO ₂ equivalent of materials.	34

Table 2.12.	Cost of materials.	34
Table 3.1.	Slump values.	35
Table 3.2.	Fresh Densities.	36
Table 3.3.	Compressive strength test results.	37
Table 3.4.	Flexural strength test results.	38
Table 3.5.	Cohesive, initial crack, and unstable fracture toughness values of mixtures.	39
Table 3.6.	Dynamic modulus of elasticities calculated from resonance frequency tests results.	42
Table 3.7.	Volume of permeable pore space (voids, %) calculated from water absorption tests readings.	45
Table 3.8.	Initial and secondary rates of absorption for six different mixtures at two different ages (28 th day and 90 th day).	48
Table 3.9.	Percentage of mass losses due to impact and abrasion.	51
Table 3.10.	Freeze thaw durability factor.	53
Table 3.11.	Ultimate load capacities for given thicknesses.	55

LIST OF SYMBOLS

a	Crack length
a_0	Initial crack length
a_{eff}	Effective crack length
b	Width / thickness
C_i	Initial compliance
d	Height / depth
d	Effective depth
E	Modulus of elasticity
f_{ck}	Characteristic concrete cylinder compressive strength
f_{ctk}	Concrete flexural tensile strength
h	Thickness of slab
H_0	Thickness of knife-edge used to fix the clip gauge
k	Modulus of subgrade reaction
KIC^c	Cohesive fracture toughness
KIC^{ini}	Initial cracking toughness
KIC^{un}	Unstable fracture toughness
l	Radius of relative stiffness
P_{max}	Maximum load
s	Specimen loading span
S	Span length
u_0	Length of the perimeter of the loaded area based on the effective dimensions of the baseplate
u_1	Length of the perimeter at a distance 2d from the loaded area
ν	Poisson's ratio, taken as 0.2
γ_c	Factor of safety of concrete
τ	Tyre pressure

LIST OF ACRONYMS/ABBREVIATIONS

CCP	Coal Consumption Products
CMOD	Crack Mouth Opening Displacement
CTOD	Crack Tip Opening Displacement
ECC	Engineered Cementitious Composites
GWP	Global Warming Potential
HVFAC	High Volume Fly Ash Concrete
OPC	Ordinary Portland Cement
RCC	Roller Compacted Concrete
SSC	Self-Compacted Concrete
W/B	Water To Binder Ratio

1. INTRODUCTION

Due to the increase in human population and energy usage, reducing the consumption of energy and natural resources, as well as CO₂ emission has become one of the greatest challenges of today's world. Reducing CO₂ emission is a focusing object all around the world due to global warming. Paris Agreement, European Green Deal, and Kyoto Protocol are some of the international agreements that aim to reduce environmental pollution.

Since the construction industry is responsible for a considerable amount of the world's CO₂ emissions, various actions are taken to make the construction materials and methods sustainable. Concrete is one of the main sources of CO₂ mainly because of the cement it contains. Cement production is responsible for approximately 6% of overall CO₂ emission worldwide [1].

The cement production process causes a high amount of CO₂ emission due to two main reasons which are chemical reactions and fossil fuel consumption. In the chemical reaction to produce lime from limestone, reactants are calcium carbonate (CaCO₃) and heat, products are calcium oxide (CaCO) and carbon dioxide (CO₂) [2]. The first source of CO₂ emission caused by cement production can be explained by the chemical reaction happening while producing lime. It is a known fact that high temperatures are required in order to produce cement both for producing lime and reacting it with silica, aluminum, and iron-containing materials. Fossil fuel consumption in order to achieve these high temperatures can be considered as the second reason for the CO₂ emission of cement production [2].

Replacement of cement with pozzolanic materials is considered as one of the most efficient and practical ways to reduce the environmental impact of concrete, and there are a variety of pozzolanic materials available around the world (fly ash, slag, silica fume, etc.).

In the scope of this study, fly ash was used to partially replace the cement. Fly ash is a waste material from coal consumption. According to the “European Green Deal”, recovering secondary raw materials from wastes is an encouraging subject. Fly ash usage in concrete has a triple effect for increasing sustainability: decreasing the use of cement and environmental pollution as well as enhancing some properties of concrete. Increased level of replacement further decreases environmental damage made by the production of concrete if targeted performance parameters could be obtained.

The spherical and smooth surface of fly ash particles usually improves the workability of concrete [3]. However, the use of fly ash as cement replacement material usually decreases the strength of concrete, especially in the early ages, which is mainly due to its slower reaction rate of it. Lam *et al.*, (2000) indicated the reducing effect of fly ash on the compressive strength is especially higher for higher water to binder (W/B) ratios [4]. In another study, it was shown that it is possible to achieve high strength with fly ash replacement up to 60% at a lower W/B ratio, regardless of whether fly ash was class F or class C [5].

In this study, the performance of high volume fly ash concrete (HVFAC) with two different replacement levels (40-60%) and two different W/B ratios (0.35-0.50) were measured experimentally, and the results were compared with the control mixtures without fly ash. Therefore, a total of 6 mixtures were designed and tested.

Then, by using the material properties obtained for 6 mixtures, the structural design of an industrial floor was made, based on TR34. Lastly, environmental impact and cost analysis was done for all concrete series. Then, the materials were compared by means of required thickness, environmental impact, and cost.

This study was a comprehensive study that includes fresh state properties, strength properties, durability properties, and economical and environmental analysis of high volume fly ash concrete. It differs from previous studies by including different perspectives while studying HVFAC. Also, there was no previous study for freeze thaw

durability of pumpable HVFAC. This study also included freeze thaw durability of conventional HVFAC.

1.1. What is the Origin of Fly Ash?

40% of global energy was produced by coal-burning at the beginning of the 21st century [6]. There are several coal consumption products (CCP) due to burning pulverized coal in thermal plants. And fly ash is one of these CCPs. There is also bottom ash, boiler slag, and flue gas as CCP. Fly ash is collected with the help of a mechanical separator or electrostatic precipitators [7].

The total annual coal consumption product (CCP) production is about 800Mt [6], according to 2010 figures. Most of this CCP obtained is fly ash, which is around 70% of the total [8].

Different types of coals such as lignite, sub-bituminous and bituminous coals, and anthracite may be used to heat water to drive the steam generators that convert thermal energy into electricity. The total amount of ash that is obtained from thermal power plants may change from 6% to 40% (by mass) of coal used. Anthracites have 6% - 15% ash and lignites have 20% - 40% ash [7]. Approximately 650000t fly ash and bottom ash is obtained from a typical 1000MW thermal power plant, annually [7].

Fly ash is a fine graded solid material with a particle size range of 0.2-200 μm . The particle size of fly ash mostly depends on the particle size of coal used and the collection procedure used. When mechanical separators are used, coarser fly ash is obtained than fly ash obtained with electrostatic precipitators.

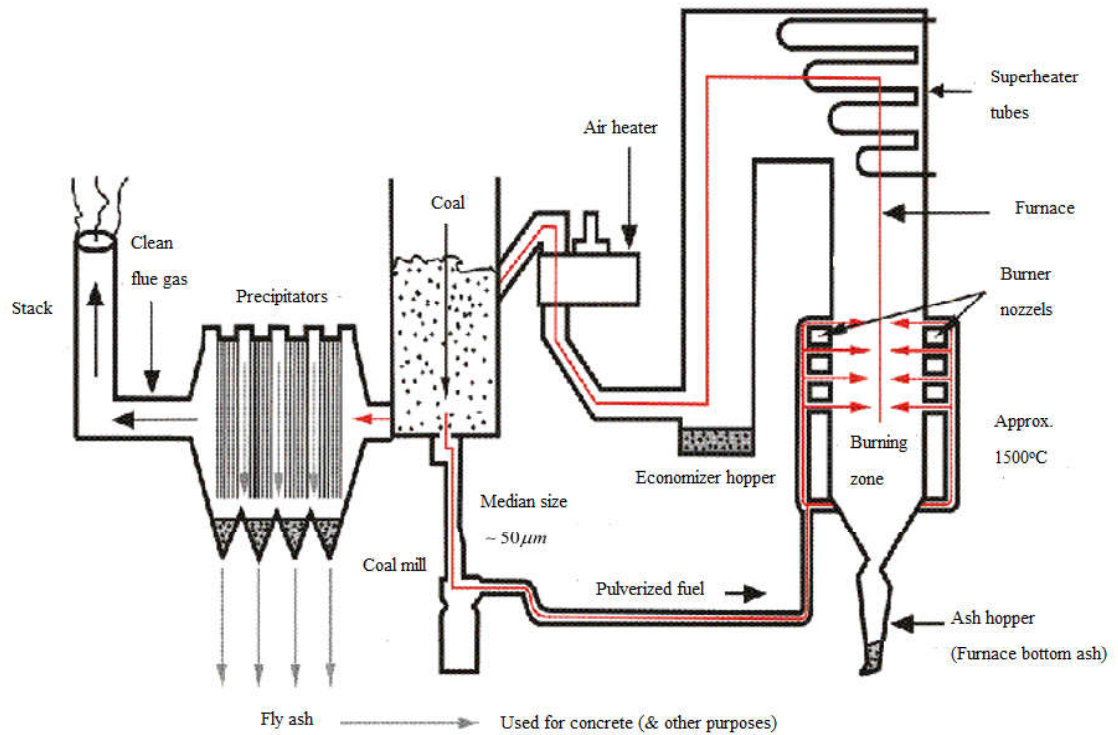


Figure 1.1. Fly ash collection processes at thermal power plant [9].

Mostly, fly ashes contain silica (SiO_2), alumina (Al_2O_3), iron oxide (Fe_2O_3), and magnesia (MgO) more than 85% of it. Fly ash from the combustion of lignite and sub-bituminous coals contains more lime than fly ash from bituminous coals and anthracite [7].

The chemical composition of fly ash varies according to the type and amount of impurities present in the coal. While fly ashes obtained from anthracite were usually rich in silica, alumina, and iron oxide, fly ashes produced as a residue from lignite may contain significant amounts of lime and sulfur trioxide in addition to formers. The fly ashes obtained from bituminous and sub-bituminous coals, generally result in between these two [7]. The chemical composition of fly ash is also affected by the composition method and collection method.

Table 1.1. Chemical composition of fly ash according to the coal it is obtained [10].

%	Anthracite	Bituminous	Subbituminous	Lignite
SiO₂	47 - 68	7 - 68	17 - 58	6 - 45
Al₂O₃	25 - 43	4 - 39	4 - 35	6 - 23
Fe₂O₃	2 - 10	2 - 44	3 - 19	1 -18
CaO	0 - 4	1 - 36	2 - 45	15 - 44
MgO	0 - 1	0 - 4	0.5 - 8	3 - 12
Na₂O	-	0 - 3	-	0 - 11
K₂O	-	0 - 4	-	0 - 2
SO₃	0 - 1	0 -32	4 - 16	6 - 30

1.2. Classification of Fly Ash

1.2.1. Early Classification According to SiO₂, Al₂O₃, CaO, and SO₃ Content

There are three groups in the early classification of fly ash. The first group is silicoaluminous, which contains mostly SiO₂ and Al₂O₃ and obtain from the combustion of anthracite and some bituminous coals. Sulpocalcic fly ashes are rich in SO₃ and CaO and are usually obtained from lignites of lower calorific value. Fly ashes containing a high amount of SiO₂ and CaO are called silicocalcic and are obtained from sub-bituminous coals and lignites [7].

And also, a similar classification specifies fly ash in four groups as Type I, II, III, and IV. The four types of fly ash content can be found in Table 1.2.

Table 1.2. Classification of fly ash as Type I, II, III, and IV [11].

	Amount %			
Constituent	Type I	Type II	Type III	Type IV
SiO ₂	> 50	35-50	<35	Very low
Al ₂ O ₃		High		
Fe ₂ O ₃		Medium		
Al ₂ O ₃ + Fe ₂ O ₃	Medium			
CaO	<7	More than Type I	Very high	Very high

1.2.2. According to CaO Content

According to CaO content fly ash is classified as low lime fly ash and high lime fly ash. While low lime fly ash has CaO content in a lower percentage than 10%, high lime fly ash contains more than 10% CaO. High lime fly ashes possess some cementitious value in addition to pozzolanic property while low lime fly ashes only have pozzolanic property [12].

There are two important standards which are ASTM C618 and EN197-1 that effected by this classification type.

ASTM C618-12 defines fly ash in two groups which are class F fly ashes and class C fly ashes. In this study class F fly ash will be used, which is the type of fly ash that requires the sum of SiO₂, Al₂O₃, Fe₂O₃ content more than 70% and is generally obtained from anthracite or bituminous coals. Class C fly ashes are mostly obtained from lignites or sub-bituminous coals. This type of fly ashes requires the sum of SiO₂, Al₂O₃, Fe₂O₃ content more than 50% and some of them may contain more than 20% CaO [13].

EN 197-1 also dived fly ashes in two groups as siliceous (V) and calcareous (W). At least 25% of siliceous fly ashes mass should be reactive SiO₂ and at most 18% of

its mass should be reactive CaO. And calcareous fly ash is the type of fly ash at least 25% of its mass should be reactive SiO₂ and at least 18% of its mass should be reactive CaO [14].

1.3. Fly Ash Use in Concrete

Fly ashes usually show pozzolanic character which is discovered as early as the 1910s. They also show both pozzolanic and latent hydraulic properties, in case of high lime content. This information has led to their use as an important ingredient in concrete since the 1930s [7].

Class F fly ash which is the type of fly ash that will be used in this study contributes to the strength of concrete with secondary hydration reaction to produce secondary CSH. Secondary CSH is produced with the reaction of CH in concrete with SiO₂ in fly ash to produce CSH which is a stronger element than CH [15]. The equation given below shows the secondary hydration reaction $3 \text{Ca(OH)}_2 + 2 \text{SiO}_2 + \text{H}_2\text{O} = 3\text{CaO} \cdot 2\text{SiO}_2 \cdot 3\text{H}_2\text{O}$ [15].

1.3.1. EN 206 Instruction for Fly Ash in Concrete

EN 206 standard specifies that the maximum amount of fly ash used in concrete should be taken as 33% of cement amount by mass. If used in greater amounts, the extra part is considered as a filler. Standard also specifies the calculation of equivalent cement amount for the concrete that includes pozzolanic materials as the summation of cement amount and k times pozzolan amount. In fly ash case k can be taken as 0.2 for CEM I 32.5 cement and 0.4 for CEM I 42.5 and higher types of cement. Equivalent cement amount is taken into account while checking minimum cement content and maximum W/B ratio [16].

In literature for HVFAC, the k value mostly was not considered. Since the standards always stay in the conservative area and staying in this area could be an obstacle

to see the effect of replacement of cement with fly ash in high amount. In the study of Sen Du *et al.* [17], and also in the study of Zhifang Zhao *et al.* [18] k value was not taken into consideration while designing concrete.

1.3.2. Literature Review

The use of fly ash as pozzolanic material in concrete was reported in 1914 for the first time [19]. However, the first comprehensive study was made in 1937 at California University by Davi and his coworker [20].

There are many studies about fly ash in literature. However, no studies were found for freeze thaw durability of pumpable HVFAC. In this study freeze thaw durability of HVFAC was examined as a comprehensive study. Fresh state properties, hardened state properties which are strength and durability properties of HVFAC was tested and calculated. From the properties obtained from these tests, an industrial floor was designed for each concrete mixture. For these industrial floors, analyses were made from both economic and environmental perspectives. In this method, the aim is to show the effects of high volume fly ash replacement in a real scenario.

1.3.2.1. Fresh State Properties. Fly ash replacement with cement improves the workability and flowability. In this study, for all concrete mixtures, 160-180 mm slump value range was targeted in order to obtain pumpable concrete to represent real time situation for industrial floors. To achieve these slump values, a modified polycarboxylate base superplasticizer was used. The effect of fly ash replacement on workability was interpreted according to the change in needed superplasticizer amount. In the study by Paulo Ricardo de Matos *et al.*, improvement of flowability of SCCs could be also observed in a reduction in superplasticizer contents [21]. This was probably the result of the spherical shape and surface smoothness of fly ashes, which can decrease the friction between particles in the mixture.

1.3.2.2. Strength Properties. In the results of the study by Qian Huang *et al.* about the behavior of cement paste with high volume fly ash, compressive strengths at 7 days were 28.2 MPa and 14.8 MPa, respectively for OPC pastes and pastes with 50% fly ash replacement ratio. However compressive strengths at 28 days were found out as 46.9MPa and 30.5 MPa respectively. These results also showed that the compressive strength of pastes decreases with the replacement of cement with fly ash. However, the difference between compressive strengths of paste 50% fly ash and paste without fly ash, was smaller at later ages [22].

In the study conducted by P. Jiang and his colleague, the compressive strength of concrete decreased with the increase in the fly ash volume, even when their curing temperature history is different. However, concrete with the same fly ash dosage had different compressive strength in decreasing order as outdoor curing, temperature matched curing, steam curing, and standard curing [23].

When the high volume fly ash concrete exposed to high temperature was considered, concrete with 90% fly ash ratio at 400, 600, 800°C had the lowest level of compressive strength, and concrete with 30% fly ash ratio at 800°C temperature had the highest level of compressive strength in the Yu, Jim *et al.* study. This also showed that higher fly ash ratios result in lower compressive strength and at lower fly ash ratios higher temperatures result in higher strength [24].

It was also seen that the water/binder ratio was effective in compressive strength reduction of fly ash addition in the Lam *et al.* study. In this study, 25% fly ash replacement does not have a significant negative effect even at 7 days at a lower W/B ratio. At a W/B ratio of 0.24, 45% fly ash replacement ratio caused an 8% decrease in compressive strength at 28 days. However, with 0.3 W/B ratio and 55% fly ash replacement ratio resulted in a 28% reduction, and with 0.5 W/B ratio and 55% fly ash replacement resulted in a 38% reduction at 28 days compressive strength [25].

In the study of Yu *et al.* when fly ash/binder ratio was lower than 60%, and in very low water/binder ratio; very high strength could be achieved regardless of fly ash is class C or class F. However, for the 80% fly ash replacement ratio, concrete with class C fly ash had slightly higher strength than concrete with class F fly ash, and for the 96%, fly ash ratio concrete with class C showed a higher strength development rate. Since class C fly ash has a much higher calcium content, it reacts earlier than class F fly ash [5].

Also, there are some studies about engineered cementitious composites (ECC) with high volume fly ash content. In a study, it was observed that the compressive strength of ECC mixtures was decreased by about 17-20% when the fly ash to binder ratio increased up to 70%. This might be related to class F fly ash would act as a filler and reduce the chemical bond development in the matrix due to its low CaO content [26].

In another research about high volume fly ash in engineered cementitious composites, showed that the addition of fly ash resulted in a reduction in compressive strength from ECC without fly ash. Also, the compressive strength gaining rate of composites with high volume fly ash was less than composites without fly ash, at 28 days. However, at 90 days composites with 40% and 60% fly ash ratios exhibited gain in compressive strength with 28 days compressive strength of composites without fly ash. While testing for compression, fracture mechanism in composites with and without fly ash are found out as similar [27].

In a study by Mohamed Sherir *et al.*, it was seen that when the change in the bending capacity was more than 43%, the change in flexural strength was significantly lower, about 25%, regardless of fly ash content. It is also seen that increasing the fly ash/cement ratio to 2.2 from 1.2 strongly influenced the bending capacity of the ECC mixture [26].

Flexural strength of ECC mixtures without fly ash has higher flexural strength than ECC mixtures with high volume fly ash at 28 days in Arun Kumar Ammasia *et al.* study. However, when curing was increased to 90 days, the flexural strength of the mixture with 40% fly ash increases up to 7% and it is similar for mixture with 60% fly ash. When the replacement of fly ash increased from 80% to 100%, the flexural strength decreased. Arun Kumar Ammasia *et al.* study also showed that ECC increased the ductility regardless of the presence of fly ash [27].

In the study conducted by Mohamed A.A. Sherir *et al.*, high volume fly ash ECC showed lesser splitting tensile strength than composite without fly ash at 28 days. However, when curing was increased to 90 days, composites with 40% and 60% replacement levels showed similar strength to composite without fly ash [26].

In the study conducted by Grzegorz Ludwik Golewski, low calcium fly ash concrete with 20% and 30% fly ash ratios was examined. At the age of 28 days, the control specimen and concrete with 20% fly ash have similar fracture toughness values, and concrete with a 30% fly ash ratio has a lower fracture toughness value. At the age of 90 days, concrete with a 20% fly ash ratio has the highest fracture toughness while concrete with 30% fly ash has the lowest fracture toughness value. In this study fracture toughness showed similar changes with compressive strength while specimens getting age [28]. It should be stated that this study is about low calcium fly ash concrete, not HVFAC.

At 28 days, with increasing fly ash level, there was a decrease in modulus of elasticity in the study of P. R. de Matos *et al.* Only with one fly ash type, which was the one indicating better mechanical performance in compression, did not represent negative effect up to 60% replacement level. To not observe negative effects for other fly ashes, the replacement level should have remained less than 40% [21]. Also, in another study, it could be seen that, with increasing replacement level of fly ash, modulus of elasticity decreased [26].

All of the above studies showed that strength properties are affected by fly ash replacement levels, W/B ratios and the age of specimens since pozzolanic reactions of fly ash occur at later ages. In this study strength properties of specimens were examined for two different fly ash replacement ratios, two different W/B ratios and at two different ages in order to see the effect of these factors. And the strength properties for all mixtures at all ages were used for the design and were evaluated from different perspectives. Also, the fracture toughness of six different mixtures was calculated for both ages. The difference of this study is it examined the fracture toughness of concrete with high fly ash replacement ratios.

1.3.2.3. Durability Properties. Jiang *et al.* showed that the porosity of concrete would decrease up to 50% replacement level but increased at higher replacement levels [21]. In another study, it is also seen that the addition of 50% fly ash, increased the pore volume within every pore size classification [22].

The water absorption test in the study conducted by A. K. Ammasi and Ragul resulted that with increasing fly ash replacement, water absorption of ECC decreased. Which is compatible with porosity results [27]. In another study sorptivity increases with an increase in the replacement ratio of cement with fly ash [24].

In the study conducted by Ali Mardani-Aghabaglou *et al.*, freeze thaw durability of roller compacted concrete (RCC) as HVFAC was investigated. The study shows that freeze thaw durability of concrete decreases with the replacement of cement with fly ash. On the other hand, the addition of fly ash without removing cement results in an increment in freeze thaw durability. Also, this study has a parallel result in the water absorption test that is porosity increment with fly ash replacement and decrease in porosity with the addition of fly ash [29].

One of the main targets of this study is to examine the freeze thaw durability of HVFAC since there is a gap in the literature for this property. Porosity is one of the main reasons for freeze thaw damage, and comments can be made on porosity with the

water absorption and sorptivity properties of the mixture. This is why in this study, water absorption and sorptivity tests were conducted along with a rapid freeze thaw damage test. Also, this study was examined the length change and abrasion behavior of specimens since freeze thaw damage is mostly seen on roads and, these two properties are also important for the durability of concrete pavements.

1.3.2.4. Analysis. 85% of the CO₂ emission of concrete production is from Portland cement production. So, the increase in the cement replacement level of fly ash reduces the mean global warming potential (GWP). In the study conducted by Paulo Ricardo de Matos *et al.*, it is seen that for 40%, 50%, and 60% fly ash content, mean GWP reduces with the increase in the fly ash level [21]. Also, approximately 70% of total coal consumption products are fly ash [7]. Since fly ash is a waste material, the replacement of fly ash with cement decreases environmental pollution while decreasing CO₂ emission due to the production of concrete due to cement use.

In this study, environmental assessments will not be done for mixtures. The analysis will be made according to the needed material amount for industrial floor design according to the same loading condition, for each mixture at each age. Also, another challenge for the convincing industry to use fly ash in high amounts is economical reasons. Economic analysis also will be made for designed floors in this study.

2. MATERIALS AND METHODS

2.1. Materials

CEM I type Portland cement, crushed stone, crushed sand and, river sand was used in all concrete series. In the high-volume fly ash concrete series, class F fly ash was used as a cement replacement material. Additionally, a superplasticizer was used as a chemical admixture, when it was necessary.

2.1.1. Cement

CEM I 42.5 R type Portland cement (according to TS EN 197-1 [14] standard) was used in this study. Its chemical, physical, and mechanical properties were given in Table 2.1, Table 2.2, and Table 2.3 respectively.

Table 2.1. Chemical properties of cement (TS EN 196-2 [30]).

Chemical Properties		Test Results
SiO ₂ Soluble (%)		18.06
Insoluble Residue (%)		0.35
Al ₂ O ₃ (%)		4.84
Fe ₂ O ₃ (%)		3.4
CaO (%)		62.7
MgO (%)		1.35
SO ₃ (%)		3.34
Loss on Ignition (%)		3.7
Cl ⁻ (%)		0.0106
Na ₂ O / K ₂ O (%)		0.24 / 0.83
S.CaO - Free lime (%)		0.8
Unknown		1.53
	C ₃ S	67.77
Mineralogical Composition	C ₂ S	0.73
	C ₃ A	7.08
	C ₄ AF	10.35
LSF		1.03

Table 2.2. Physical properties of cement (TS EN 196-3 [31] and TS EN 196-6 [32]).

Physical Properties		Test Results
Density (g/cm^3)		3.13
Initial Setting Time (min.)		131
Final Setting Time (min.)		184
Soundness (Le Chatelier) (mm)		1
Fineness	Blaine Specific Surface (cm^2/g)	3900
	Residue on $45\mu\text{m}$ sieve (%)	3.4
	Residue on $90\mu\text{m}$ sieve (%)	0.2

Table 2.3. Mechanical properties of cement (TS EN 196-1 [33]).

Mechanical Characteristic / Day	Standards (MPa)	Test Results (MPa)
Early Strength / 2 Days	≥ 20.0	30.7
Early Strength / 7 Days	-	47.9
Standard Strength / 28 Days	≥ 42.5	58.3
	≤ 62.5	

2.1.2. Fly Ash

Class F type fly ash (according to ASTM 618) was used in this study. Its chemical and physical properties were given in Tables 2.4 and 2.5 respectively.

Table 2.4. Chemical properties of fly ash (TS EN 196-2 [30] and ICP-OES).

Chemical Properties	Test Results
SiO ₂ (%)	55.38
Al ₂ O ₃ (%)	25.5
Fe ₂ O ₃ (%)	6.14
CaO (%)	2.02
MgO (%)	2.00
SO ₃ (%)	0.14
Na ₂ O (%)	0.62
K ₂ O (%)	3.80
Na ₂ O Equivalent Total Alkali (%)	3.12
TiO ₂ (%)	1.20
Cl- (%)	0.0014
Free CaO (%)	0.18
Loss on Ignition (%)	2.74

Table 2.5. Physical properties of fly ash (TS EN 450-1 [34] and TS EN 451-2 [35]).

Physical Properties	Test Results
Density (g/cm ³)	2.10
Residue on 45 μ m Sieve (%)	28.8
28 Days Pozzolanic Activity Index (%)	87.8
90 Days Pozzolanic Activity Index (%)	97.0

2.1.3. Aggregates

2 types of siliceous crushed stone, 1 type of siliceous crushed sand, and 1 type of siliceous river sand were used in this study. Physical properties (according to TS EN 1097-6 [36]) and sieve analysis (according to EN 933-1 [37]) results were given in Tables 2.6 and 2.7. The gradation curve that was prepared according to the sieve analysis

result also was given in Figure 2.1 (TS 802 [38]).

Table 2.6. Physical properties of aggregates (EN 1097-6 [36]).

Physical Properties	Crushed Stone: NO2	Crushed Stone: NO1	Crushed Sand	River Sand
Apparent Particle Density (g/cm ³)	2.79	2.78	2.71	2.69
Oven Dried Density (g/cm ³)	2.70	2.69	2.63	2.60
Saturated and Surface-Dried Density (g/cm ³)	2.72	2.71	2.67	2.63
Water Absorption (g/cm ³)	0.6	0.8	1.6	1.1

Table 2.7. Sieve analysis results of aggregates (EN 933-1 [37]).

Sieve Opening (mm)	Crushed Stone: NO2 (passing %)	Crushed Stone: NO1 (passing %)	Crushed Sand (passing %)	River Sand (passing %)
31.5	100.00	100.00	100.00	100.00
20	78.32	100.00	100.00	100.00
16	39.28	100.00	100.00	100.00
12.5	12.28	98.01	100.00	100.00
8	0.53	46.06	100.00	100.00
4	0.32	1.59	96.40	99.92
2	0.31	0.25	61.34	96.70
1	0.31	0.24	36.08	90.81
0.5	0.31	0.23	19.96	81.50
0.25	0.28	0.20	9.75	22.56
0.15	0.24	0.17	4.89	4.01
0.063	0.05	0.04	0.22	0.08

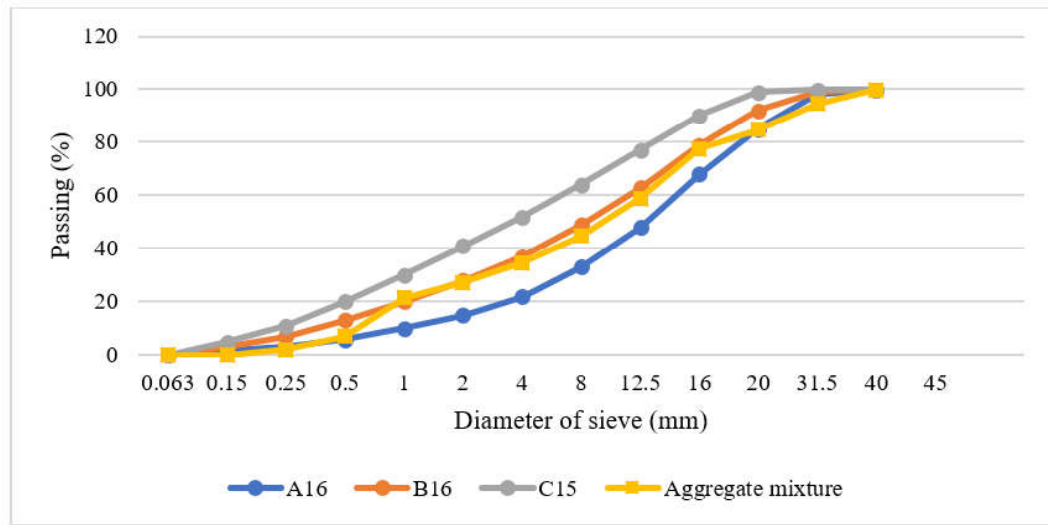


Figure 2.1. Gradation curve of the mix of aggregates with respect to reference curves (TS802 [38]).

2.1.4. Chemical Admixture

A modified polycarboxylate-based superplasticizer was used in this study to achieve a 160-180mm slump value. The density of the superplasticizer was 1.1 g/cm³.

2.2. Mixture Design

6 different mixtures were examined in this study. Mixtures with 2 different water-to-cement ratios were produced by using 40% and 60% fly ash replacement levels. Mixture notations were shown in Table 2.8.

Table 2.8. Mixture notations.

Mixture Name	Water/ Cement	Fly Ash/Binder
w 0.5 fa0	0.5	0
w 0.5 fa40	0.5	40%
w 0.5 fa60	0.5	60%
w 0.35 fa0	0.35	0
w 0.35 fa40	0.35	40%
w 0.35 fa60	0.35	60%

Firstly, aggregates and cementitious materials were mixed for 2 minutes. After the water was added in one minute while the mixer was working, then, mixtures were mixed for 3 more minutes. All mix proportions were given in Table 2.9.

Table 2.9. Mix proportions.

Mixture	Cement (kg)	Fly Ash (kg)	Water (kg)	No.2 (kg)	No.1 (kg)	Crushed Sand (kg)	Natural Sand (kg)	SP (kg)
w 0.5 fa0	420	0	210	443	529	435	342	0.84
w 0.5 fa40	252	168	210	420	502	412	325	0.42
w 0.5 fa60	168	252	210	410	490	403	317	0.00
w 0.35 fa0	420	0	147	471	563	462	364	4.20
w 0.35 fa40	252	168	147	450	539	442	348	3.36
w 0.35 fa60	168	252	147	435	521	427	337	2.94

2.2.1. Specimen Curing

All specimens were cured in the mold for 1 day and they were kept in the curing tank until their 28th day. Specimens that were tested at age 90 days, were air cured between days 28 and 90. The temperature of water in the curing tank was set at around $20 \pm 2^\circ\text{C}$ according to EN 12390-2 [39][39] standard.

2.3. Experimental and Calculating Methods

2.3.1. Fresh State Tests

2.3.1.1. Slump Test. Slump tests were performed according to EN 12350-2 [40]. The slump cone was filled with concrete in 3 layers. Each layer was approximately $\frac{1}{3}$ of the volume of the cone and each layer was rodded 25 times uniformly.



Figure 2.2. Slump test.

2.3.1.2. Fresh State Density Test. Density test performed according to EN 12350-6 [40] standard. Mold with 5-liter volume was filled with concrete in 2 layers and it was compacted with a vibration table. Mass of the mold with and without concrete was recorded and the density of concrete was calculated.

2.3.2. Strength Tests

2.3.2.1. Compressive Strength Test. Cylinder specimens with a diameter of 100 mm and a height of 200 mm were tested according to EN 12390-3 [39] standard. Specimens were loaded with a 0.6 MPa/s loading rate. Six specimens were tested for each mixture. 3 of the specimens were tested at the age of 28 days and the other 3 specimens were tested at the age of 90 days.



Figure 2.3. Compressive strength test.

2.3.2.2. Three-Point Bending Test. Load controlled 3-point bending test applied to 100*100*500 mm³ specimens at 28th days and 90th days according to the JCI-S-001 [41] standard to obtain flexural strength of materials. For each mixture, 3 specimens were tested.

Crack mouth opening and applied load data were collected from the experiments to calculate fracture parameters and flexural strength.

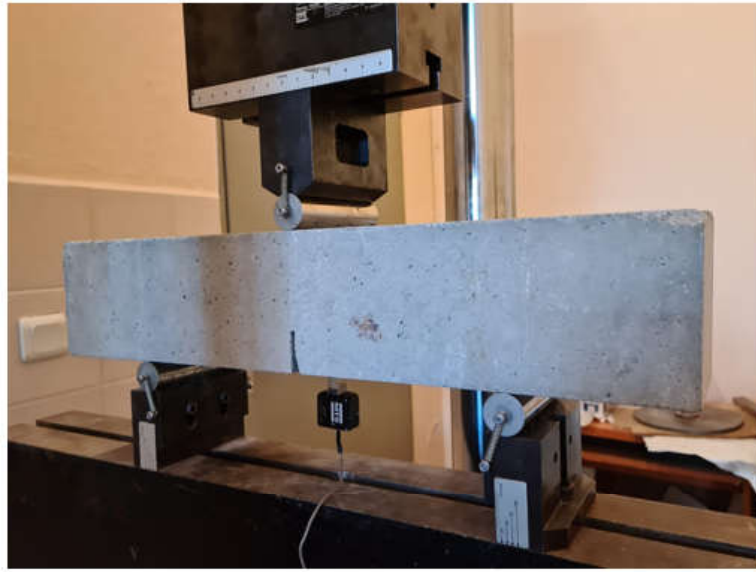


Figure 2.4. Three-point bending test.

2.3.2.3. Fracture Parameter Calculation. The specimens that were conducted three point bending test according to JSI-S-001 [41] were analyzed for their fracture behavior. There are two important material parameters which are unstable fracture toughness (K_{IC}^{un}) and initial cracking toughness (K_{IC}^{ini}). These two parameters are important in order to designate the state of the crack. Until fracture toughness of material reaches initial cracking toughness, it can be said that elastic deformation occurs at the specimen. When fracture toughness is equal to initial cracking toughness, it means that crack initiates. In the situation that fracture toughness is more than initial cracking toughness but smaller than unstable fracture toughness, it can be said that crack propagates stably. And at last, when fracture toughness of material became more than unstable fracture toughness, unstable crack propagation occurs [42].

Unstable fracture toughness was calculated based on linear elastic fracture mechanics assumptions [43] and initial cracking toughness was calculated double K fracture parameters method [44]. In order to use, double K fracture parameters method, cohesive fracture toughness (K_{IC}^c) need to be calculated. In this study, it was calcu-

lated with the help of weight function [45] [44]. All formulas that were used are:

$$K_{IC}^{ini} = K_{IC}^{un} - K_{IC}^c, \quad (2.1)$$

$$K_{IC}^{un} = \frac{3 * P_{max} * S * \sqrt{a_{eff}}}{2 * b * d^2} * f\left(\frac{a_{eff}}{d}\right), \quad (2.2)$$

where

$$f\left(\frac{a_{eff}}{d}\right) = \frac{1.99 - \frac{a_{eff}}{d} * \left(1 - \frac{a_{eff}}{d}\right) * [2.15 - 3.93 * \frac{a_{eff}}{d} + 2.7 * \left(\frac{a_{eff}}{d}\right)^2]}{\left(1 - 2 * \frac{a_{eff}}{d}\right) * \left(1 - \frac{a_{eff}}{d}\right)^{1.5}}, \quad (2.3)$$

where P_{max} is the maximum load (N), S is the span length (m), d is the height (m), b is the width (m), a_{eff} is the effective crack length,

$$a_{eff} = \frac{2}{\pi} (d + H_0) * \arctan \sqrt{\frac{B * E * (CMOD_c)}{32.6 * P_{max}}} - 0.1135 - H_0, \quad (2.4)$$

where d is the depth (m), B is the thickness (m), H_0 is the 1.75mm, the thickness of knife-edge used to fix the clip gauge, $CMOD_c$ is the crack mouth opening displacement at maximum load, E is the modulus of elasticity,

$$E = \frac{6 * S * a_0 * V_I(\alpha_0)}{C_i * b * d^2}, \quad (2.5)$$

where S is the specimen loading span, a_0 is the initial crack length, C_i is the initial compliance,

$$V_I(\alpha_0) = 0.76 - 2.28\alpha + 3.87\alpha^2 - 2.04\alpha^3 + \frac{0.66}{(1 - \alpha)^2} \quad (2.6)$$

$$\alpha_0 = \frac{a_0 + H_0}{d + H_0}, \quad (2.7)$$

and

$$\begin{aligned}
K_{IC}^c = & \frac{2}{\sqrt{2*\pi*a}} * [A_1 * a [2 * s^{0.5} + M_1 * s + \frac{2}{3} * M_2 * s^{1.5} \\
& + \frac{M_3}{2} * s^2 + \frac{2}{3} * M_4 * s^{2.5}] + A_2 * \\
& a^2 [\frac{4}{3} s^{1.5} + \frac{M_1}{2} * s^2 + \frac{4}{15} * M_2 * s^{2.5} + \frac{4}{35} * M_4 * s^{3.5} \\
& + \frac{M_3}{6} * \left(1 - \left(\frac{a_0}{a}\right)^3 - 3 * s * \frac{a_0}{a}\right)]]
\end{aligned} \tag{2.8}$$

where a is the crack length, a_0 is the initial crack length,

$$s = 1 - \frac{a_0}{a}, \tag{2.9}$$

$$A_1 = \sigma_u * CTOD_c, \tag{2.10}$$

$$A_2 = \frac{f_t - \sigma_u * CTOD_c}{a - a_0}, \tag{2.11}$$

where σ_u is the equivalent stress due to the maximum load, a_c is the at peak load,

$$CTOD_c = CMOD_c * \left[\left(1 - \frac{a_0}{a_c}\right)^2 + \left(1.081 - 1.149 * \frac{a_0}{D}\right) \left[\frac{a_0}{a_c} - \left(\frac{a_0}{a_c}\right)^2\right] \right]^{0.5}. \tag{2.12}$$

Universal weight function parameters are:

$$M_i = a_i + b_i * \frac{a}{D}, \quad i = 2 \text{ and } 4, \tag{2.13}$$

$$\begin{aligned}
M_i = & \frac{1}{\left(1 - \frac{a}{D}\right)^{1.5}} * [a_i + b_i * \frac{a}{D} + c_i * \left(\frac{a}{D}\right)^2 \\
& + d_i * \left(\frac{a}{D}\right)^3 + e_i * \left(\frac{a}{D}\right)^4 + f_i * \left(\frac{a}{D}\right)^5], \quad i = 1 \text{ and } 3,
\end{aligned} \tag{2.14}$$

where D is the depth of beam.

The constant a_i , b_i , c_i , d_i , e_i , f_i , and calculate M_i values can be found in Table 2.10.

Table 2.10. The constants a_i , b_i , c_i , d_i , e_i , f_i , and calculate M_i values [45].

i	a_i	b_i	c_i	d_i	e_i	f_i	M_i
1	-0.0008	0.6879	0.4943	-3.2542	3.4427	-1.369	0.5047
2	0.7823	-3.0489					-0.4963
3	-0.3049	13.4187	-23.3166	35.5107	-34.4410	14.1034	6.6870
4	0.2835	-7.3784					-2.8108

2.3.3. Durability Tests

2.3.3.1. Resonance Frequency Test. All specimens that were tested for flexural strength and fatigue performance were also tested using a resonance frequency test device and dynamic moduli were calculated. This test was performed according to the ASTM C215-14 [46] standard. Masses and every dimension of specimens were measured. Then the resonance frequencies of the specimens were recorded to calculate dynamic elastic modulus.

Freeze-thaw specimens were also tested with a longitudinal resonance frequency test device in every reading. These readings were taken in every (at most) 36 freeze-thaw cycles.

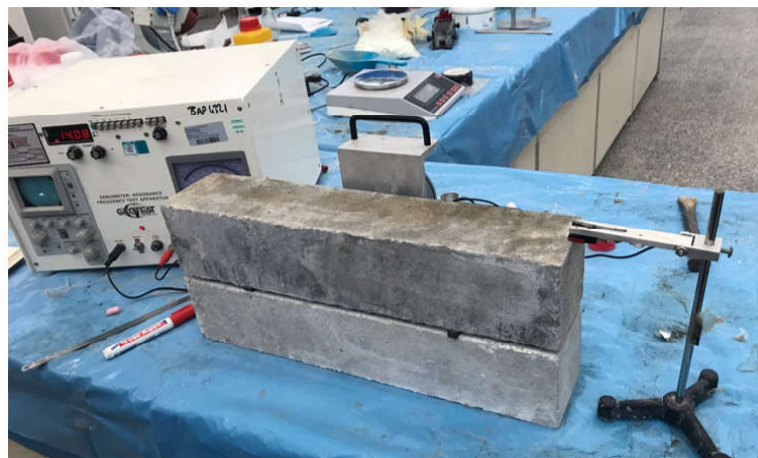


Figure 2.5. Longitudinal resonance frequency test.

2.3.3.2. Water Absorption Test. Permeable water absorption capacity of specimens was determined according to ASTM C642-13 [47]. Three specimens were tested at the age of 28 days and 3 specimens were tested at the age of 90 days for each of the 6 mixtures. 50 mm height specimens were cut from 100 mm height cylindrical specimens to obtain specimens with a volume of more than 350 cm³.

Specimens were kept in an oven at a temperature of $110 \pm 5^\circ\text{C}$ for not less than 24 hours (Figure 2.6-a). They were weighed with 24 hours period until the weight change was less than 0.5% between two successive values. The lowest value was designated as oven-dry mass (A).

Oven-dry specimens were kept in the water with a temperature of approximately 21°C for not less than 48 hours (Figure 2.6-b). Masses of the surface dried specimens were measured every 24 hours until the weight change was less than 0.5% between two successive values. The highest value was designated as saturated mass after immersion (B).

Saturated specimens were boiled for 5 hours and waited to cool with natural loss of heat for not less than 14 hours (Figure 2.6-c). After cooling, surface dried weights of specimens were designated as saturated mass after boiling (C).

Lastly, specimens were weighed in water, and results were designated as immersed apparent mass (D) (Figure 2.6-d).



Figure 2.6. Water absorption test stages- (a) oven drying procedure (b) saturation after immersion procedure (c) saturation after boiling procedure (d) immersed apparent mass procedure.

2.3.3.3. Sorptivity Test. Sorptivity test applied according to ASTM C1585-13 [48] standard. To obtain the water absorption rate of mixtures, 6 cylindrical specimens for each mixture with 100 mm diameter and 50 ± 3 mm height were prepared (3 specimens for testing at an age of 28 days, and 3 specimens for testing at an age of 90 days). The specimens tested at 90 days (which were kept in air after the 28th day) were saturated according to the vacuum-saturation process in ASTM C 1202 [49] standard.

Saturated specimens both at age 28 days and 90 days were weighed and placed in the desiccator with a saturated solution of potassium bromide inside an oven at

a temperature of 50°C for 3 days. After 3 days, specimens were placed in separate sealable containers and waited for at least 15 days at $23 \pm 2^{\circ}\text{C}$ before the beginning of the absorption procedure.

After 15 days, conditioned specimens were weighed, and 4 diameters were measured from the side which will be in contact with water. After measuring them, specimens' side faces were sealed with paraffine, and top surfaces were closed with a plastic bag loosely. Sealed specimens were also weighed, and measured weights were recorded at the nearest 0.01g.

Testing containers were filled with water so that the water level will be 1-3 mm above the support devices. The water levels were kept constant in these intervals during the absorption process. Mass of specimens was recorded at 60 ± 2 seconds, 5 minutes ± 10 seconds, 10 ± 2 minutes, 20 ± 2 minutes, 30 ± 2 minutes, 60 ± 2 minutes after placing the test surface of the specimen on the support device. The measurements were taken every hour, ± 5 minutes, up to 6 hours. Specimens were measured for their masses once a day for up to 3 days. 3 more measurements at least 24 hours apart were taken between day 4 and day 7. Final measurements were taken at least 24 hours later from the measurement on the 7th day. Specimens were measured after surface water was removed with a wet cloth.



Figure 2.7. Sorptivity test.

2.3.3.4. Length Change Test. Length change of specimens was measured according to ASTM C157/C157M - 17 [50] standard. The length of specimens was measured for initial CRD, which is the difference between the comparator reading of the specimen and the reference bar at any age after they waited in the lime-saturated water at $23 \pm 0.5^\circ\text{C}$ for a minimum of 30 minutes after de-molding at age 1 day. After 28 days of curing in the lime-saturated water at $23 \pm 2^\circ\text{C}$, second comparator readings were taken. From the age of 28 days, specimens were air-stored as it is stated in the ASTM C490 [51] standard. Specimens were stored in a cabinet with $50 \pm 4\%$ relative humidity at $23 \pm 2^\circ\text{C}$. Readings were taken at 4, 7, 14, and 28 days, and 8, 16, 32, 64 weeks after curing according to ASTM C490 [51] standard.



Figure 2.8. Length change measurement.

2.3.3.5. Abrasion Test. Mixtures' potential resistance to damage by impact and abrasion was determined according to ASTM C1747/1747M-13 [52] standard. 3-cylinder

specimens with 100 mm diameter and 100 mm height were included in the test for each mixture both for the 28th day and 90th day. Specimens were placed in the Los Angeles machine and the machine rotated for 500 revolutions with the rate of 30 to 33 rotation/minute. These 3 specimens were weighed together, before and after the procedure.



Figure 2.9. Abrasion test.

2.3.3.6. Freeze-Thaw Test. Freeze-thaw durability test was proceeded according to ASTM C666/C666M - 15 [53] standard. Test procedures were started at the age of 90 days. All specimens were measured for all 3 dimensions. Masses and resonance frequencies of every specimen were recorded at approximately 4 °C and water saturated. Specimens were placed at the cabinet and freeze thaw cycles from -18°C, to 4°C were applied. Masses and resonance frequencies of specimens were measured at every 36 cycles, mostly, until 300 cycles were completed.



Figure 2.10. Freeze-thaw test.

2.3.4. Design and Analysis

2.3.4.1. Thickness Design of Industrial Floor. Ground supported slab designs were made for all mixtures with the properties both at the age of 28 days and 90 days according to TR34 [54] (4th edition) for single point load. Chosen thicknesses were checked for both bending capacity and punching shear capacity by using the following formulas and materials properties.

Bending capacity for an internal load is calculated as,

$$P_{u,0} = 2 * \pi * (M_p + M_n) \quad \text{for } a/l = 0, \quad (2.15)$$

$$P_{u,0.2} = \frac{4 * \pi * (M_p + M_n)}{1 - \left(\frac{a}{3l}\right)} \quad \text{for } a/l = 0.2. \quad (2.16)$$

Bending capacity for an edge load is calculated as,

$$P_{u,0} = \frac{\pi * (M_p + M_n)}{2} + 2 * M_n \quad \text{for } a/l = 0, \quad (2.17)$$

$$P_{u,0.2} = \frac{\pi * (M_p + M_n) + 4 * M_n}{1 - \left(\frac{2a}{3l}\right)} \quad \text{for } a/l = 0.2, \quad (2.18)$$

where a is the equivalent radius of contact area of the load, l is the radius of relative stiffness, M_n is the negative (hogging) resistance moment of the slab (kNm), taken to be that of the plain unreinforced concrete, M_p is the ultimate positive (sagging) resistance moment of the slab (kNm), taken to be that of the reinforced concrete,

$$a = \sqrt{\frac{P}{\pi * \tau}}, \quad (2.19)$$

$$l = \sqrt[4]{\frac{E * h^3}{12 * (1 - \mu^2) * k}}, \quad (2.20)$$

$$M_n = \frac{f_{ctk} * h^2}{\gamma_c * 6}, \quad (2.21)$$

where M_p is the 0 since no reinforcement used, P applied load, τ is the tyre pressure (N/mm², k modulus of subgrade reaction (N/mm²/mm, taken as N/mm³), E is the modulus of elasticity of the concrete (N/mm²), ν is the Poisson's ratio, taken as 0.2, f_{ctk} is the concrete flexural tensile strength (taken as average of the flexural strength of three specimens in this study), $\gamma_c = 1.5$ for concrete.

Since the modulus of elasticity of specimens were not measured in the scope of this study, and the values are required to determine the thickness of floors, the modulus of elasticity values were estimated by using the compressive strength values of the mixtures, by using the TS 500 [55] equation given as,

$$E = 3250 * \sqrt{f_{ckj}} + 14000. \quad (2.22)$$

For shear at the face of the loaded area,

$$P_{p,max} = \nu_{max} * u_0 * d, \quad (2.23)$$

$$\nu_{max} = 0.5 * k_2 * f_{cd}, \quad (2.24)$$

where

$$f_{cd} = \frac{f_{ck}}{\gamma_c}, \quad (2.25)$$

$$k_2 = 0.6 * \left(1 - \frac{f_{ck}}{250}\right). \quad (2.26)$$

For shear on the critical perimeter,

$$P_p = \nu_{Rd,c} * u_1 * d, \quad (2.27)$$

$$\nu_{Rd,c} = 0.035 * k_s^{1.5} * f_{ck}^{0.5}, \quad (2.28)$$

$$k_s = 1 + \left(\frac{200}{d}\right)^{0.5} \leq 2, \quad (2.29)$$

where, f_{ck} is the characteristic concrete cylinder compressive strength (taken as an average of the compressive strength of three specimens in this study), u_0 is the length of the perimeter of the loaded area based on the effective dimensions of the baseplate, d is the effective depth (0.75*h for unreinforced concrete), u_1 is the length of the perimeter at a distance 2d from the loaded area, h is the thickness of slab.

2.3.4.2. Environmental Analysis of the Industrial Floor. In order to calculate the CO₂ emission of a 2000 m² industrial floor, the volume of material was determined that will be needed to construct the industrial floor. Then the CO₂ equivalents for materials (Table 2.11) in concrete were obtained from “The Inventory of Carbon and Energy Database v3.0” [56] of Bath University. From these data, CO₂ equivalents for all mixtures were calculated for a 2000 m² slab by multiplying the unit CO₂ equivalent with

the amount of material that will be used for each material and summing up the CO₂ equivalent from all materials.

Table 2.11. CO₂ equivalent of materials.

	Cement	Fly Ash	Water	No.2	No.1	Crushed Sand	Natural Sand	SP
kg CO₂ e/ kg	0.912	0.004	0.00034	0.00438	0.00438	0.00438	0.00904	1.88

2.3.4.3. Economic Analysis of the Industrial Floor. While calculating the cost of a 2000 m² slabs, prices taken from a local trader were used for each ingredient of material (Table 2.12). Also, current allowance prices for CO₂ equivalents were taken into account according to the “EU Emissions Trading System (EU ETS)” [57] report. The total volume needed for the 2000 m² industrial floor was already calculated in order to determine CO₂ equivalent. By using these volumes cost for all materials was calculated, and allowance price for calculated CO₂ emission was also added to the total cost.

Table 2.12. Cost of materials.

	Cement	Fly Ash	Water	No.2	No.1	Crushed Sand	Natural Sand	SP
\$ / kg	0.03226	0.01267	0.00092	0.00472	0.00472	0.00472	0.00593	0.51843

3. RESULTS AND DISCUSSION

3.1. Fresh State Test Results

3.1.1. Slump Test Results

All specimens for all six mixtures were poured with three mixing procedures. For all mixing procedures, slump values were measured. The target slump value was between 16 cm and 18 cm. Table 3.1 shows all measurements for the slump test. According to the table, all mixtures achieved with the targeted value of slump.

Table 3.1. Slump values.

	Slump (cm)		
w 0.5 fa0	18	16	17
w 0.5 fa40	17.5	18	17.5
w 0.5 fa60	17	18	18
w 0.35 fa0	18	17	18
w 0.35 fa40	16.5	16.5	17.5
w 0.35 fa60	16.5	18	18

3.1.2. Fresh Density Test Results

Fresh densities were measured, and results can be seen in Table 3.2. Measured densities were compatible with the theoretical densities that are calculated from mixture proportions. From Table 3.2, it can be seen that the density of concrete was increased with the decreasing W/B ratio. This situation can be explained by increasing the aggregate amount per volume with the decreasing water content. Since aggregate has a higher density, its mass was higher than the same volume of water.

Table 3.2 also shows that increasing fly ash replacement leads to a decrease in density. This is an expected outcome since cement was directly replaced with the same amount of fly ash and the density of fly ash is lesser than cement. Also, fly ash with the same weight represents more volume and this situation leads to less aggregate in the same volume. Less aggregate and cement, more fly ash in the same volume concludes with less density since the fly ash has a lower density than cement and aggregate.

Table 3.2. Fresh Densities.

Mixture Name	Fresh Densities (kg/L)
w 0.5 fa0	2.38
w 0.5 fa40	2.29
w 0.5 fa60	2.25
w 0.35 fa0	2.43
w 0.35 fa40	2.35
w 0.35 fa60	2.29

3.2. Strength Test Results

3.2.1. Compressive Strength Test Results

Three specimens were tested for each mixture in order to determine the compressive strength of concrete mixtures according to BS EN 12390-3 [39] for both at age of 28 days and 90 days. Average compressive strength for all six mixtures for both 28 days and 90 days were given with their standard deviations in Table 3.3 and Figure 3.1.

Table 3.3. Compressive strength test results.

Mixtures	28 Days		90 Days	
	Compressive Strength (MPa)	Standard Deviation	Compressive Strength (MPa)	Standard Deviation
w 0.5 fa 0	36	0.78	55.8	2.16
w 0.5 fa 40	25.7	0.67	37.7	0.71
w 0.5 fa 60	16.3	2.65	22	1.06
w 0.35 fa 0	50.3	1.9	75	1.26
w 0.35 fa 40	36.9	2.86	57.9	0.94
w 0.35 fa 60	24.2	1.14	38.5	1.03

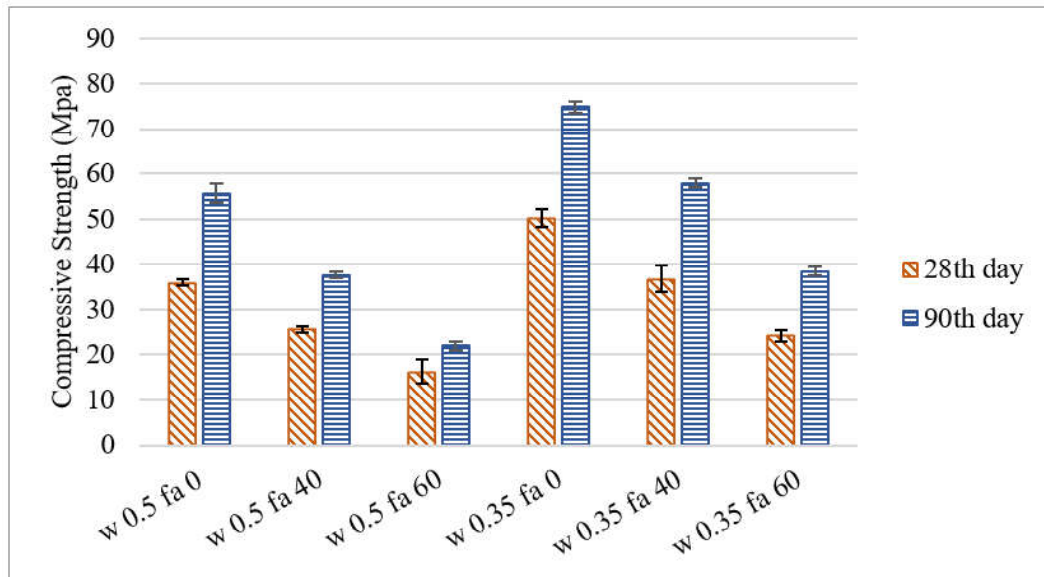


Figure 3.1. Compressive strength test results.

It can be clearly seen that the compressive strength of mixtures decreased with both replacement of fly ash and increasing in w/b ratio from Figure 3.1. It can be also seen that compressive strength decrease due to fly ash replacement can be compensated with decreasing of w/b ratio at the age of 28 days. When “w 0.5 fa 0 - w 0.35 fa 40” and “w 0.5 fa 40 - w 0.35 fa 60” mixture pairs were investigated, the mixtures in the pair have similar compressive strength at the age of 28 days. However, when these mixture pairs were examined at the age of 90 days, it can be concluded that mixtures with higher fly ash replacement ratios gain more strength by means of compression.

Compression test results also show that the reduction in strength by replacement with fly ash occurs at lower percentages in lower W/B ratio, especially in higher fly ash replacement which is compatible with Lam *et al.*, 2000 study [25].

3.2.2. Three-Point Bending Test Results

Three point bending tests were performed for each mixture in order to determine the flexural strength of concrete mixtures according to JCI-S-001 [41] standard for both at age of 28 days and 90 days. Test results for both 28 days and 90 days were given in Table 3.4 and Figure 3.2.

Table 3.4. Flexural strength test results.

Mixtures	28 Days		90 Days	
	Flexural Strength (MPa)	Standard Deviation	Flexural Strength (MPa)	Standard Deviation
w 0.5 fa 0	4.87	0.17	6.96	0.41
w 0.5 fa 40	4.15	0.12	6.16	0.37
w 0.5 fa 60	3.15	0.35	3.98	0.24
w 0.35 fa 0	7	0.41	7.81	0.45
w 0.35 fa 40	5.17	0.09	7.04	0.48
w 0.35 fa 60	4.1	0.12	5.83	0.76

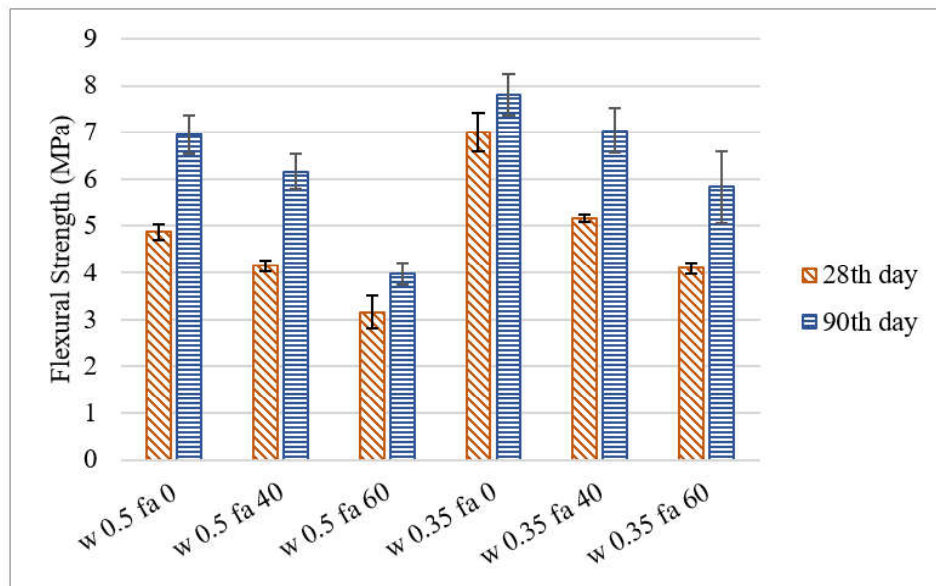


Figure 3.2. Flexural strength test results.

Based on the results given in Figure 3.2, lower flexural strength values were found for the mixtures with a high W/B ratio, as expected. Additionally, flexural strength values were found to decrease with increasing fly ash replacement ratios. At the age of 90 days, all mixtures had gained strength substantially. For mixtures with 0.35 W/B ratio, it is also clearly seen that the flexural strength of the specimens with a 40% fly ash replacement ratio almost reached the flexural strength of control specimens at the age of 90 days.

3.2.3. Fracture Analysis from Three Point Bending Test

Specimens tested according to JSI-S-001 [41] standard for three point bending test examined according to their fracture behavior. From the data that were obtained from tests, cohesive toughness of concretes was calculated with weight function[45] and initial cracking toughness was found with the difference between unstable fracture toughness and cohesive fracture toughness according to the double K parameter method [44]. They can be found in Table 3.5.

Table 3.5. Cohesive, initial crack, and unstable fracture toughness values of mixtures.

		K_{IC}^c (MPa \sqrt{m})	K_{IC}^{un} (MPa \sqrt{m})	K_{IC}^{ini} (MPa \sqrt{m})
28th day	w 0.5 fa 0	0.3532	0.8257	0.4725
	w 0.5 fa 40	0.2808	0.6949	0.4141
	w 0.5 fa 60	0.2174	0.5266	0.3091
	w 0.35 fa 0	0.2511	1.0971	0.846
	w 0.35 fa 40	0.2504	0.8297	0.5793
	w 0.35 fa 60	0.2437	0.6735	0.4298
90th day	w 0.5 fa 0	0.3781	1.1452	0.7671
	w 0.5 fa 40	0.2622	0.987	0.7248
	w 0.5 fa 60	0.1818	0.6312	0.4494
	w 0.35 fa 0	0.4347	1.2859	0.8512
	w 0.35 fa 40	0.4917	1.2156	0.7239
	w 0.35 fa 60	0.3022	0.9533	0.6512

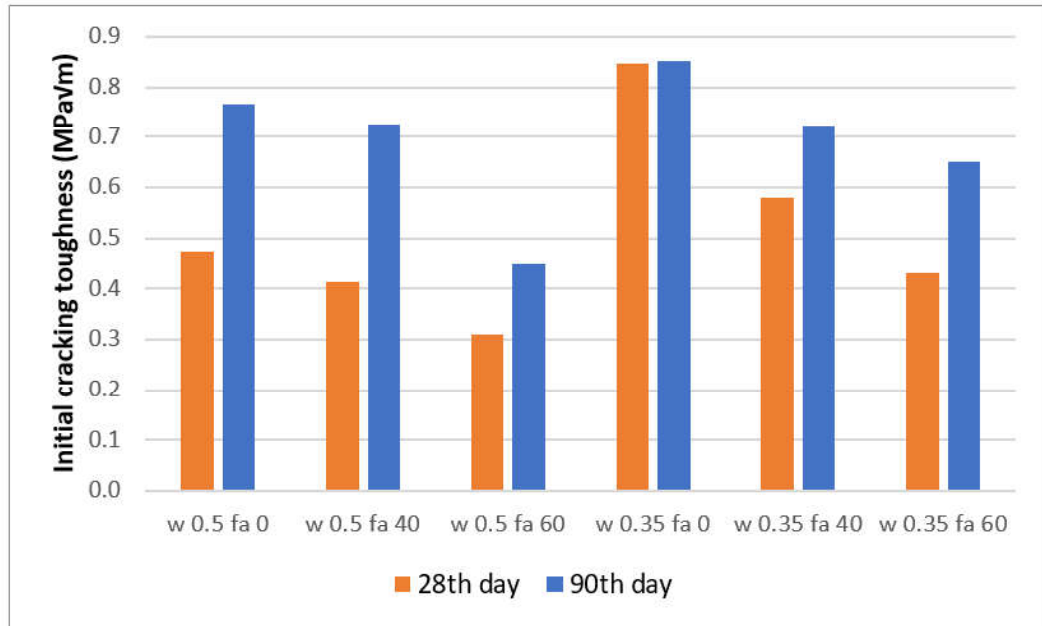


Figure 3.3. Initial cracking toughness.

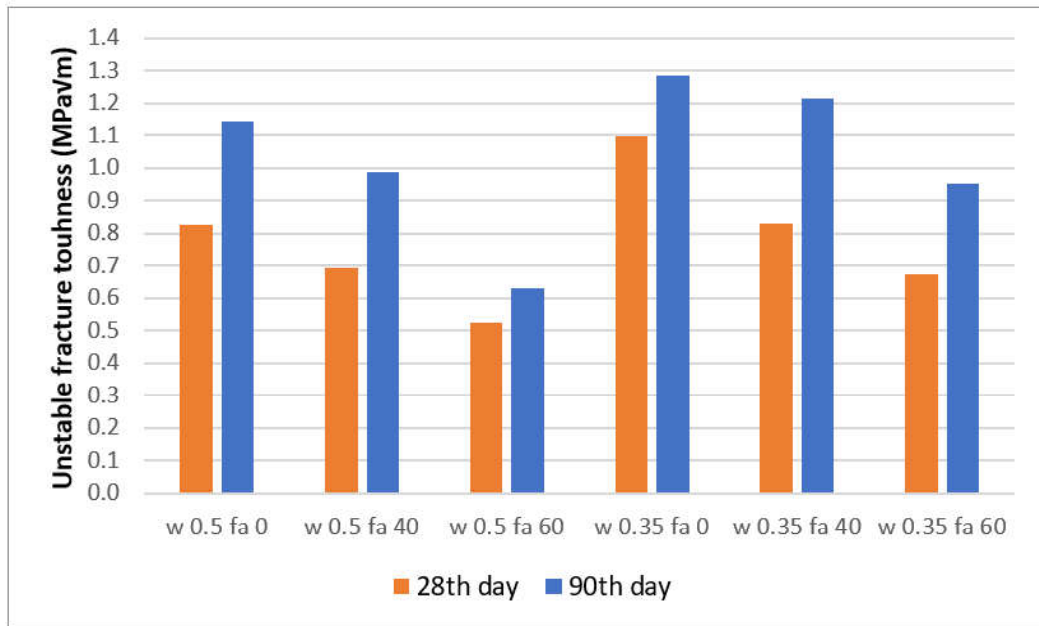


Figure 3.4. Unstable fracture toughness.

From Figure 3.3 and Figure 3.4, it is observed that both initial cracking toughness and unstable fracture toughness increased a decrease in W/B ratio. Also, while the fly ash replacement ratio was increasing, both initial cracking toughness and unstable fracture toughness were decreasing.

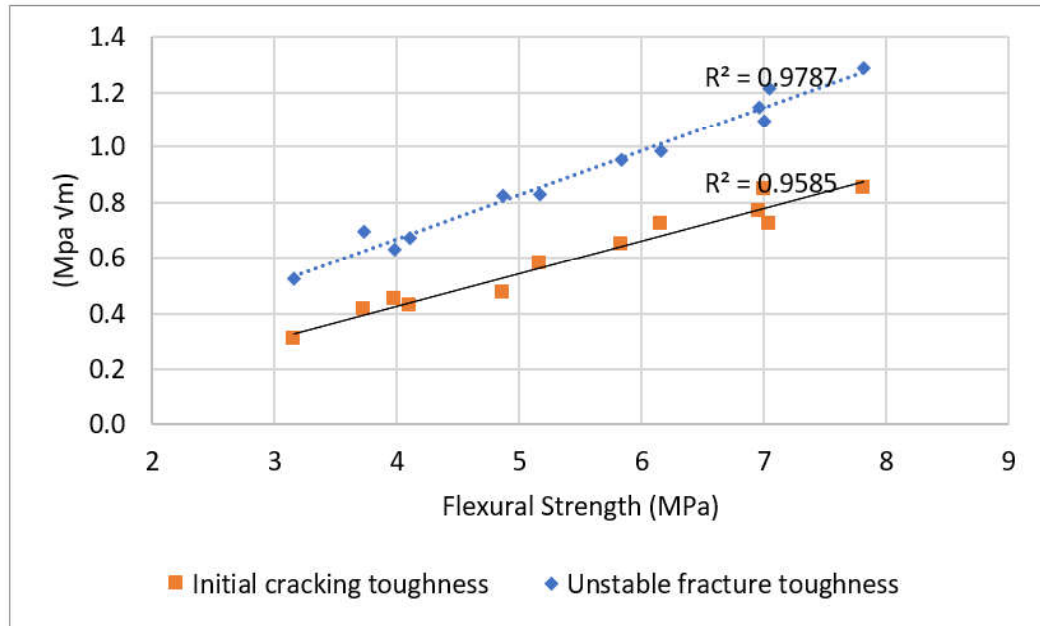


Figure 3.5. Relation between flexural strength and initial cracking toughness and unstable fracture toughness.

If the fracture toughness of concrete was smaller than the initial cracking toughness, elastic deformation continues until the crack initiates, and at the moment that they become equal crack initiates. But if fracture toughness was between initial cracking toughness and unstable fracture toughness that means the crack expands stably. When fracture toughness became the unstable fracture toughness, the crack propagation became unstable and when it exceeds unstable fracture toughness, the crack propagates unstably [42].

Higher initial cracking toughness means that the specimen shows better performance until cracking occurs while it is still in the elastic region. Higher unstable fracture toughness means that the mixture shows better performance until crack propagation became unstable. Figure 3.5 shows that there is a strong relationship between flexural strength and both initial cracking toughness and unstable fracture toughness with a very high coefficient of determination.

3.3. Durability Test Results

3.3.1. Resonance Frequency Test

Averages and standard deviations of resonance frequency test results according to ASTM C215-14 [46] can be seen in Table 3.6. For every mixture, at every age three prism specimens were tested before they were tested for flexural strength.

Table 3.6. Dynamic modulus of elasticities calculated from resonance frequency tests results.

Mixtures	28 th day		90 th day	
	Average	Standard Deviation	Average	Standard Deviation
w 0.5 fa 0	38.59	1.22	37.72	0.77
w 0.5 fa 40	34.03	0.56	33.3	1.76
w 0.5 fa 60	29.21	0.61	28.78	0.59
w 0.35 fa 0	44.76	0.29	45.7	0.81
w 0.35 fa 40	41.71	0.82	41.07	0.71
w 0.35 fa 60	37.83	0.90	38.90	1.19

It is seen that between age 28 days and 90 days there was no remarkable change in dynamic elastic modulus for all mixtures. However, it is clearly seen that increase in fly ash replacement ratio and a decrease in W/B ratio causes a decrease in dynamic elastic modulus.

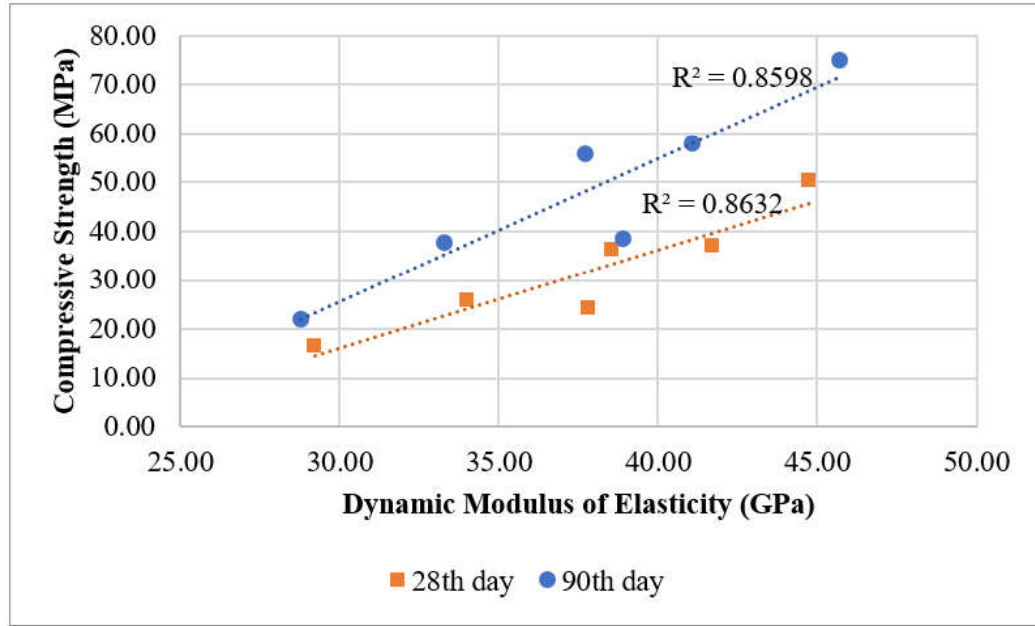


Figure 3.6. Relationship between compressive strength and dynamic modulus of elasticity calculated from resonance frequency test results.

Figure 3.6 shows that the dynamic modulus of elasticities calculated from resonance frequency test results has a strong relationship with the compressive strength of the mixture with a high coefficient of determination. It can be said that dynamic elastic modulus results have been changed parallel to change in compressive strength between mixtures at the same age.

Resonance frequency tests were applied to the specimens before the three-point bending test was applied to them. So, the specimens tested for resonance frequency and flexural strength were exactly the same specimens. In this part of the study relationship between the slope of the elastic part of the bending test results and the dynamic modulus of elasticity calculated from the resonance frequency test was investigated.

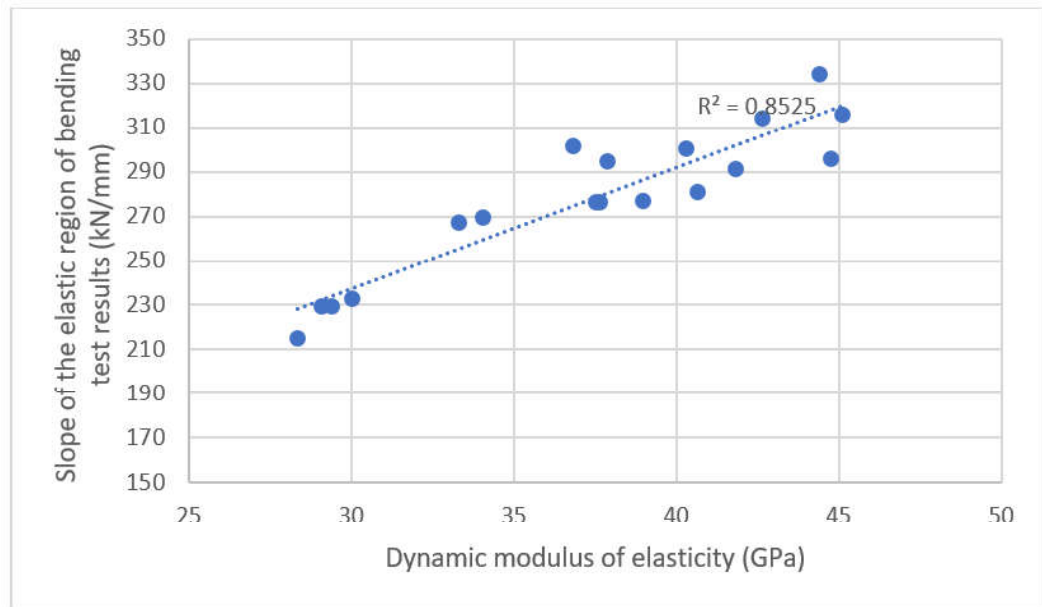


Figure 3.7. Relationship between the slope of the elastic region of bending test results and dynamic modulus of elasticity calculated from resonance frequency test results at the age of 28 days.

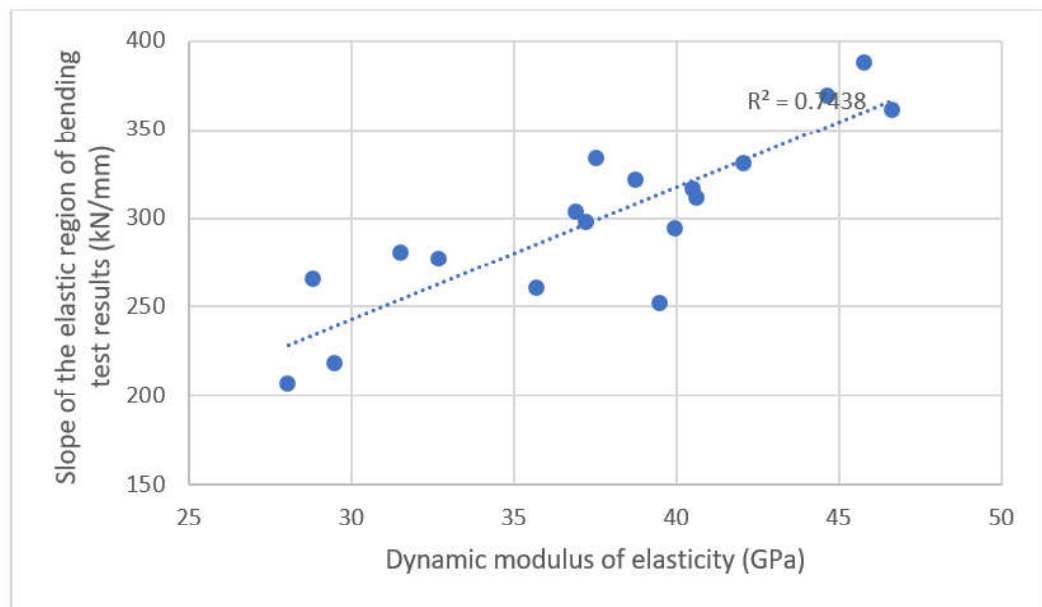


Figure 3.8. Relationship between the slope of the elastic region of bending test results and dynamic modulus of elasticity calculated from resonance frequency test results at the age of 90 days.

Figure 3.7 and Figure 3.8 show that there is a strong relationship between the dynamic modulus of elasticities calculated from resonance frequency test results and the slope of the elastic region of bending test results with a relatively high coefficient of determination at both the 28th day and 90th day. It can be said that the dynamic elastic modulus and the elastic modulus that can be calculated from the slope of the elastic region of bending tests represent the same relation between mixtures.

3.3.2. Water Absorption Test Results

Water absorption tests were applied to three specimens with a diameter of 100 mm and a height of 50 mm for each mixture according to ASTM C642-13 [47] standard. Test results can be seen in Table 3.7.

Table 3.7. Volume of permeable pore space (voids, %) calculated from water absorption tests readings.

Mixtures	28 Days		90 Days	
	Volume of permeable pore space (voids),%	Standard Deviation	Volume of permeable pore space (voids),%	Standard Deviation
w 0.5 fa 0	16.4	0.32	15.3	0.3
w 0.5 fa 40	17	0.51	16.6	0.25
w 0.5 fa 60	18.9	0.24	18.2	0.53
w 0.35 fa 0	10.6	0.3	10.5	0.42
w 0.35 fa 40	12.1	0.56	11.2	0.4
w 0.35 fa 60	13.4	0.45	13.4	0.22

Table 3.7 shows that replacing cement with fly ash caused an increase in permeable voids volume. Also, an increase in the W/B ratio led to an increase in permeable void volume percentage as expected. Voids were slightly decreased with the increasing age of specimens.

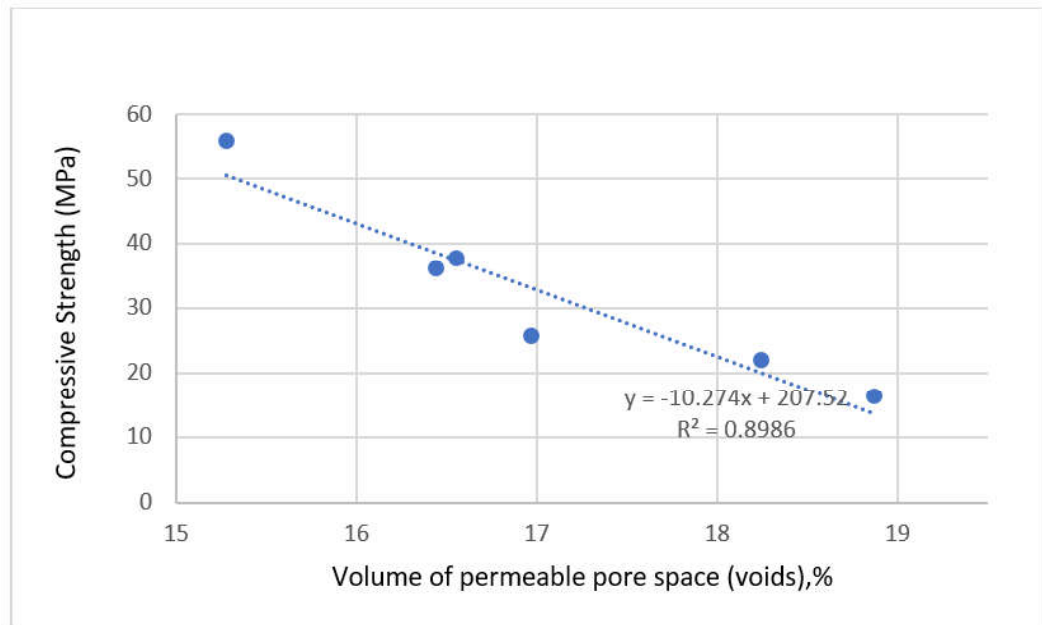


Figure 3.9. Relationship between volume of permeable pore space (voids), %, and compressive strength (MPa) for mixtures prepared with 0.5 W/B ratio.

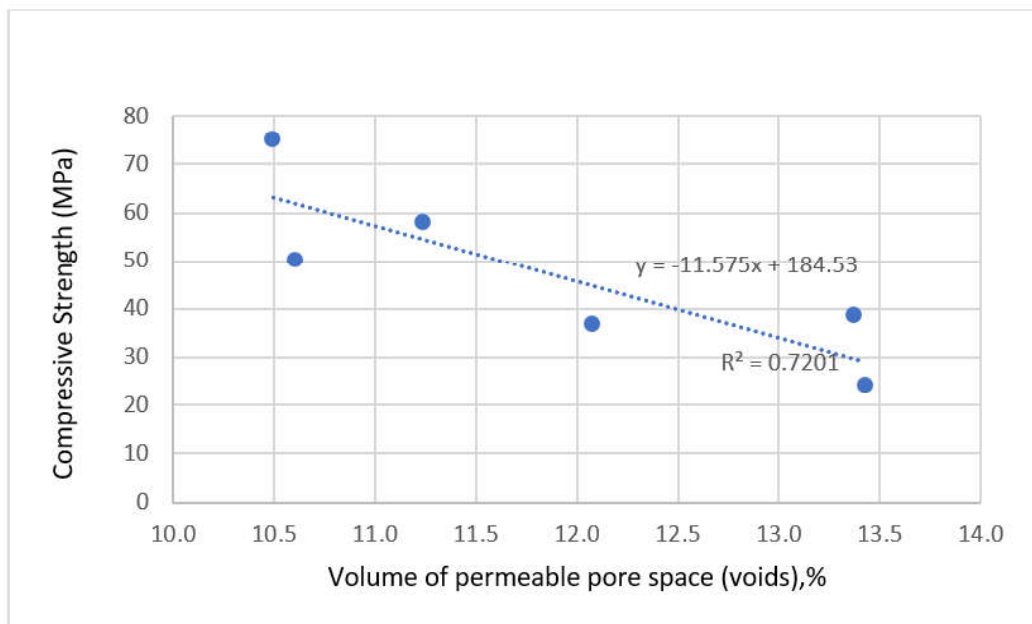


Figure 3.10. Relationship between volume of permeable pore space (voids), %, and compressive strength (MPa) for mixtures prepared with 0.35 W/B ratio.

From Figure 3.9 and Figure 3.10 it can be said that permeable pore space percentage has a relationship with compressive strength of mixture for same W/B ratio.

Replacing cement with fly ash leads to an increase in permeable voids in concrete and results with a decrease in the compressive strength for the mixtures with the same W/B ratio since voids caused discontinuities that leads to lower strength. Change in W/B ratio shifts the relation at Figure 3.9 and Figure 3.10, that is why the mixture with different W/B ratios should be considered separately. However, the slope of the trendline for the mixture with both W/B is very similar. This shows that, for the different W/B ratios, the same void ratio changes caused by fly ash have a similar effect on compressive strength.

3.3.3. Sorptivity Test

The rates of absorption of six different mixtures were calculated according to the test results that are done according to the ASTM C1585-13 [48] standard. Three cylindrical specimens with a diameter of 100 mm and a height of 50 mm were tested for every mixture at each age which are 28th day and 90th day.

According to the ASTM C1585-13 [48] standard, if the data between 1 minute and 6 hours or 1 day and 7 days do not show a linear relationship, the initial or secondary rate of absorption cannot be determined. For the 90th day data of w/c 0.35 fa 40 and w/c 0.35 fa 60, the coefficient of regression of data between 1 day and 7 days was smaller than %98. According to standard, the coefficient of regression less than 98% is interpreted as a secondary rate of absorption and cannot be determined.

Table 3.8. Initial and secondary rates of absorption for six different mixtures at two different ages (28th day and 90th day).

	Initial Rate of Absorption (mm/ \sqrt{s})		Secondary Rate of Absorption (mm/ \sqrt{s})	
	28 th day	90 th day	28 th day	90 th day
w 0.5 fa0	0.002	0.0021	0.0009	0.0011
w 0.5 fa40	0.0034	0.0048	0.0016	0.0006
w 0.5 fa60	0.0016	0.0054	0.0014	0.0005
w 0.35 fa0	0.0006	0.0008	0.0004	0.0005
w 0.35 fa40	0.001	0.0011	0.0005	CANNOT BE DETERMINED
w 0.35 fa60	0.0008	0.004	0.0005	CANNOT BE DETERMINED

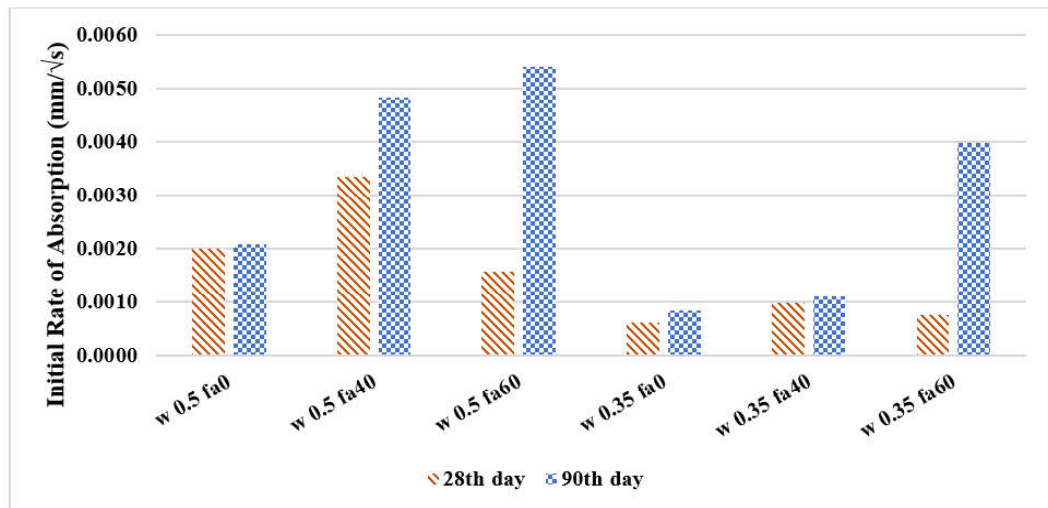


Figure 3.11. Initial rate of absorptions.

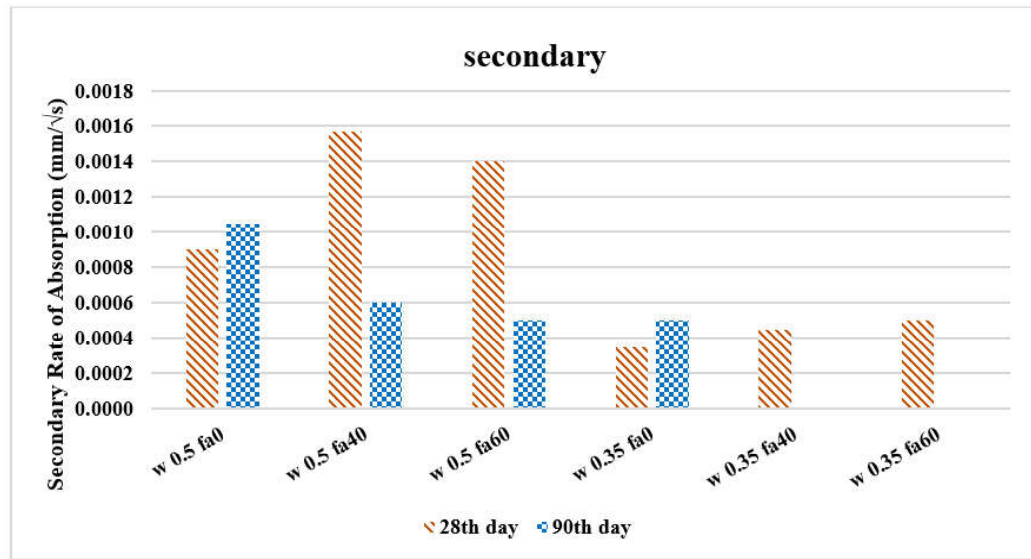


Figure 3.12. Secondary rate of absorptions.

From Table 3.8, Figure 3.11 and Figure 3.12, it is clear that mixtures with a lower W/B ratio had lower initial and secondary rate of absorption than the mixtures with a higher W/B ratio. With the increase in the W/B ratio, the void ratio was also increased according to Table 3.7. Therefore, an increment in the W/B ratio results with an increase in the rate of absorption too.

On the other hand, there was no linear relationship between fly ash replacement ratio and rate of absorption. For control mixtures with both W/B ratios, the initial and secondary rate of absorption didn't change considerably with an increase in age, since the hydration reaction of cement mostly happen in the first 28 days. However, the initial absorption rate of the mixtures, with fly ash replacement, increased with age, since secondary reaction due to fly ash occurs at later ages. With secondary reactions in concrete, voids become more capillary, and the initial rate of absorption was increased with the capillarity.

Secondary rates of absorption values for all mixtures were very smaller compared to initial rates of absorption. For the 0.5 W/B ratio, it can be said that with the fly ash replacement secondary rate of absorption was increased due to an increase in

permeable porosity. Similarly, for both fly ash replacement levels, secondary rates of absorption were decreased with age since the void ratios were decreased. For 0.35 W/B ratio, since there was no linear relationship between the data in 1 day to 7 days, no comment can be made.

3.3.4. Length Change Test

Length change of specimens was measured according to ASTM C157/C157M - 17 [50] standard. After 28 days of curing in the lime-saturated water at $23 \pm 2^\circ\text{C}$, specimens were air-stored as it is stated in the ASTM C490 [51] standard. Results of the length change test can be seen in Figure 3.13.

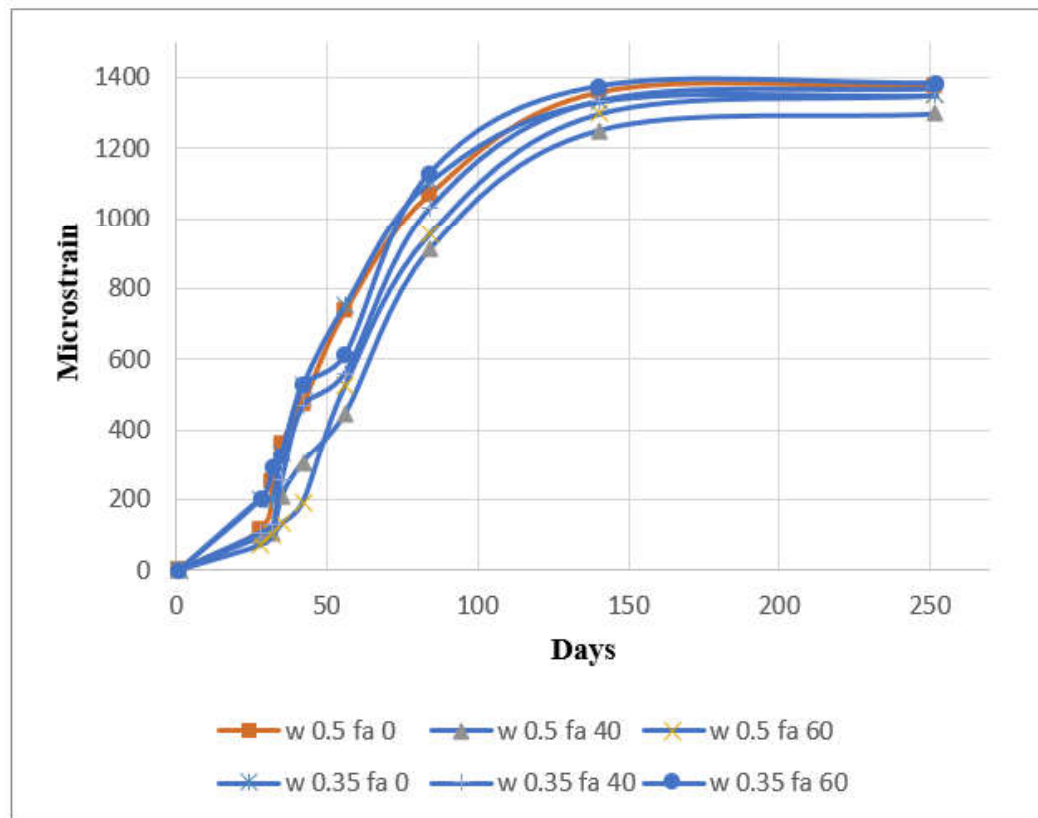


Figure 3.13. Length changes for all six mixtures.

From Figure 3.13, it is seen that there was a dramatic increase in the rate of length change after 28 days of water curing, until the 8th week at air storage. This situation was

expected since 50% humidity air storage is a more favorable environment for shrinkage to occur rather than water. After the 8th week, the rate of length change started to slow down and after the 16th week, the change in length has become nearly zero. It can be stated that most of the shrinkage has occurred in the first sixteen weeks. This behavior was similar for all mixtures. No significant difference was observed between the specimens with different fly ash replacement levels.

3.3.5. Abrasion Test

Abrasion and impact resistance of concrete mixtures for both 28th day and 90th days were determined according to ASTM C1747/1747M-13 [52] standard. Even though this standard is stated for pervious concrete, there is a study [58] in literature which was used this standard in order to determine the abrasion resistance of roller compacted concrete too.

Table 3.9. Percentage of mass losses due to impact and abrasion.

	Mass Loss (%)	
	28th day	90th day
w/c 0.5 fa0	15.6	10.7
w/c 0.5 fa40	21.9	14.6
w/c 0.5 fa60	34.7	29.1
w/c 0.35 fa0	11.8	8.7
w/c 0.35 fa40	15.6	11.2
w/c 0.35 fa60	22.2	14.6

From Table 3.9, it can be stated that increasing fly ash replacement and increasing W/B ratio results in an increase in mass loss due to impact and abrasion. Also concretes at younger ages results in a higher percentage of mass losses. No standard deviation was shared in Table 3.9 since three specimens were tested and weighted together according to the testing procedure. This procedure concludes with obtaining only one data from three specimens.

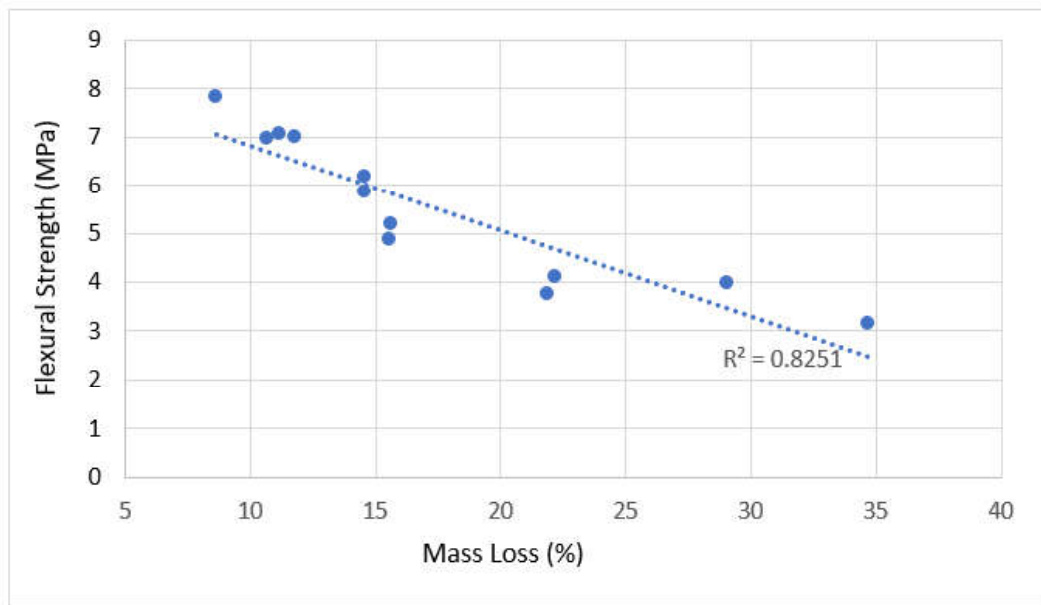


Figure 3.14. Relationship between flexural strength and mass loss which represent abrasion level of concrete.

Figure 3.14 shows that there is a strong relationship between flexural strength and mass loss due to impact and abrasion. Concrete with lower flexural strength loses more mass because of impact and abrasion. That leads to the result that concrete structures that have higher flexural strength are most likely to resist abrasion more than structures with lower flexural strength.

3.3.6. Freeze-Thaw Test

Resistance of concrete to rapid freezing and thawing cycles determined according to ASTM C666/C666M - 15 [53] standard. Relative dynamic modulus of elasticity and durability factor were calculated for all mixtures according to ASTM C215-14 [46] standard and they can be found in Figure 3.15 and Table 3.10.

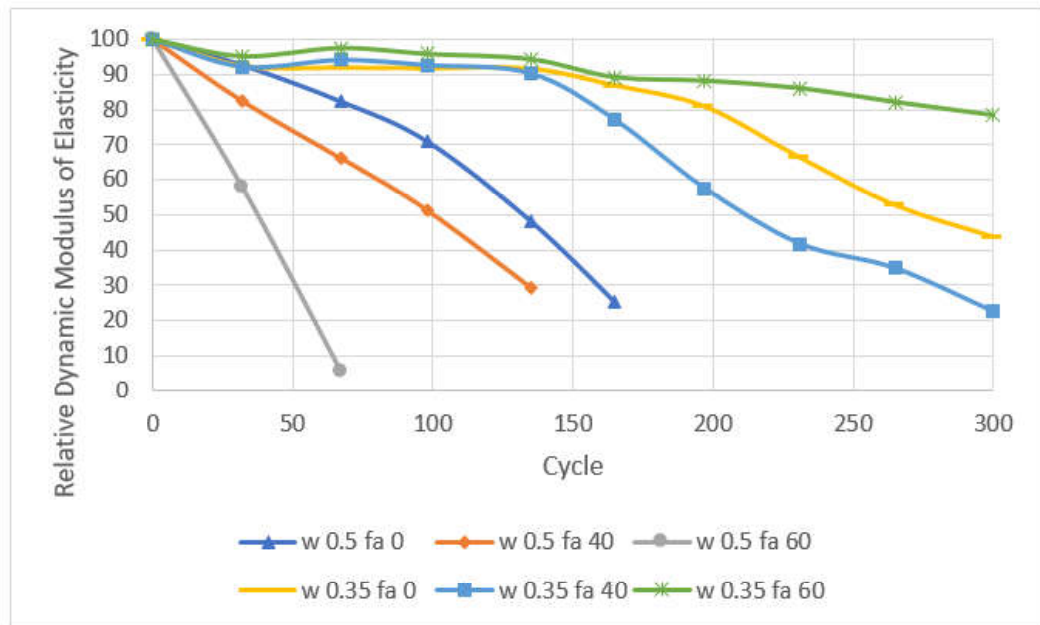


Figure 3.15. Relative dynamic modulus of elasticity.

Table 3.10. Freeze thaw durability factor.

Durability Factor	Average	Standard Deviation
w 0.5 fa 0	14	1.83
w 0.5 fa 40	13.2	0.3
w 0.5 fa 60	1.7	1.35
w 0.35 fa 0	44.1	5.46
w 0.35 fa 40	24.2	12.63
w 0.35 fa 60	78.5	3.36

For mixtures with a 0.5 W/B ratio, it can be said that increasing fly ash replacement level causes decreases in freeze thaw durability factor. Especially, with a high W/B ratio and higher fly ash replacement level, specimens showed no resistance to freeze thaw damage.

On the other hand, for the 0.35 W/B ratio, there was no meaningful relation between freeze thaw durability and fly ash replacement ratio. The mixture with the

highest freeze thaw durability was at the 60% fly ash replaced mixture. In order to understand the reason for this difference, microstructural investigations are recommended as a further study on the same specimens that will be exposed to freeze thaw cycle.

In the light of these results, it can be said that the mixture with a 0.35 W/B ratio and 60% fly ash replacement ratio showed the best resistance against freezing and thawing cycles. And mixtures with a 0.5 W/B ratio were not durable enough for freezing and thawing since they lost more than 40% of their initial dynamic modulus of elasticity before 300 cycles were completed. All mixtures with a 0.35 W/B ratio, completed 300 freeze thaw cycles. However, the best performance was achieved with a 60% fly ash replacement ratio and the worst performance was obtained with a 40% fly ash replacement ratio.

3.4. Design and Analysis

3.4.1. Thickness Design of an Industrial Floor

For all six mixtures, the thickness design of an industrial floor was made with the guidance of the TR 34 [54] report. While calculating thickness, a single point load condition was considered. Wheel load was taken as 40kN and with wheel contact dimension of 165mm*40mm from the example in TR 34 [59] (3rd edition). And modulus of subgrade reaction was taken as 0.5 N/mm³. Since wheel load is a dynamic load, the partial safety factor was taken as 1.6, and the required load capacity has been calculated as 64kN (40*1.6).

In order to find required thicknesses moment capacities and punching shear capacities were checked at critical locations. Required thicknesses and ultimate load capacities can be found in Table 3.11.

Table 3.11. Ultimate load capacities for given thicknesses.

	Mixture	h (mm)	Moment Capacity		Punching Shear Capacity	
			Pu (kN) (internal load)	Pu (kN) (edge load)	Pp,max (kN)	Pp (kN)
28 days	w 0.5 fa 0	165	158.18	64.379	312.85	174.853
	w 0.5 fa 40	180	161.469	65.336	255.047	166.502
	w 0.5 fa 60	205	161.109	64.603	192.067	159.337
	w 0.35 fa 0	140	160.783	66.414	345.998	165.538
	w 0.35 fa 40	160	157.223	64.19	309.179	169.576
	w 0.35 fa 60	180	159.602	64.615	242.23	161.744
90 days	w 0.5 fa 0	140	159.951	65.986	372.966	174.258
	w 0.5 fa 40	150	163.296	67.139	295.079	157.066
	w 0.5 fa 60	185	164.01	66.27	228.434	160.196
	w 0.35 fa 0	135	166.95	68.908	435.859	192.613
	w 0.35 fa 40	140	162.009	66.803	383.278	177.658
	w 0.35 fa 60	155	165.965	67.964	310.703	166.073

During the determination of required thickness values, it was seen that for all of the material cases moment capacities of the slabs at the edge load location were found as the most critical case.

It can be stated that the required thickness is increasing with a decrease in flexural tensile strength properties from Figure 3.16 as expected. Figure 3.16 shows the strong relationship between flexural tensile strength and thickness with a very high coefficient of determination. An increase in thickness requirement was an expected outcome. However, thickness increment not necessarily means an increase in cost or environmental impact.

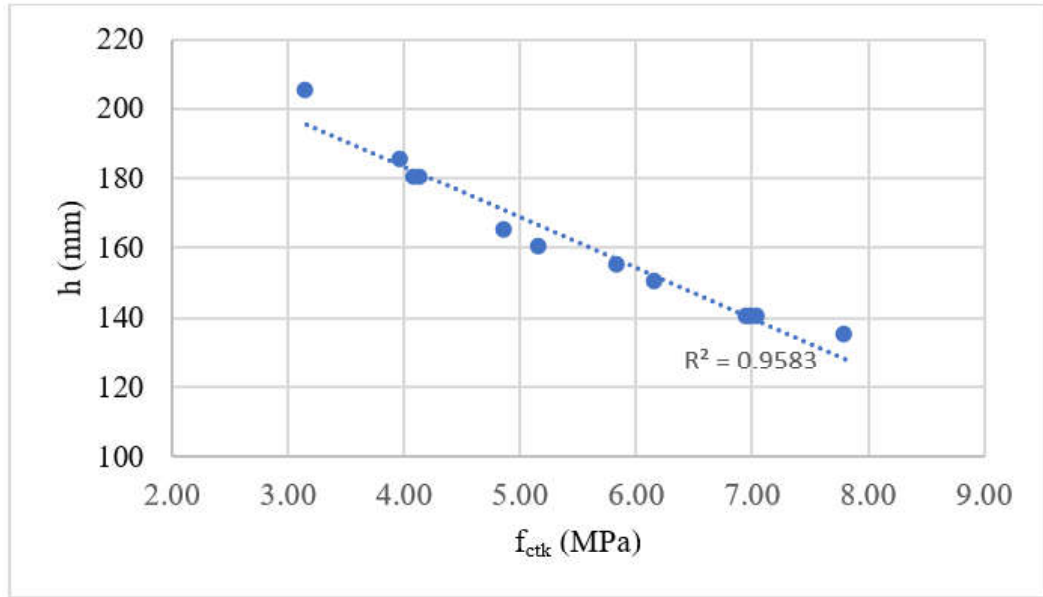


Figure 3.16. Flexural tensile strength and thickness relation.

3.4.2. Environmental Analysis for 2000 m2 Industrial Floorl

CO₂ equivalents for materials (Table 2.11) in concrete were obtained from “The Inventory of Carbon and Energy Database v3.0” [56] of Bath University. From these data, CO₂ equivalents for all mixtures were calculated for a 2000 m2 slab with the designed thickness. Results were given in Figure 3.17.

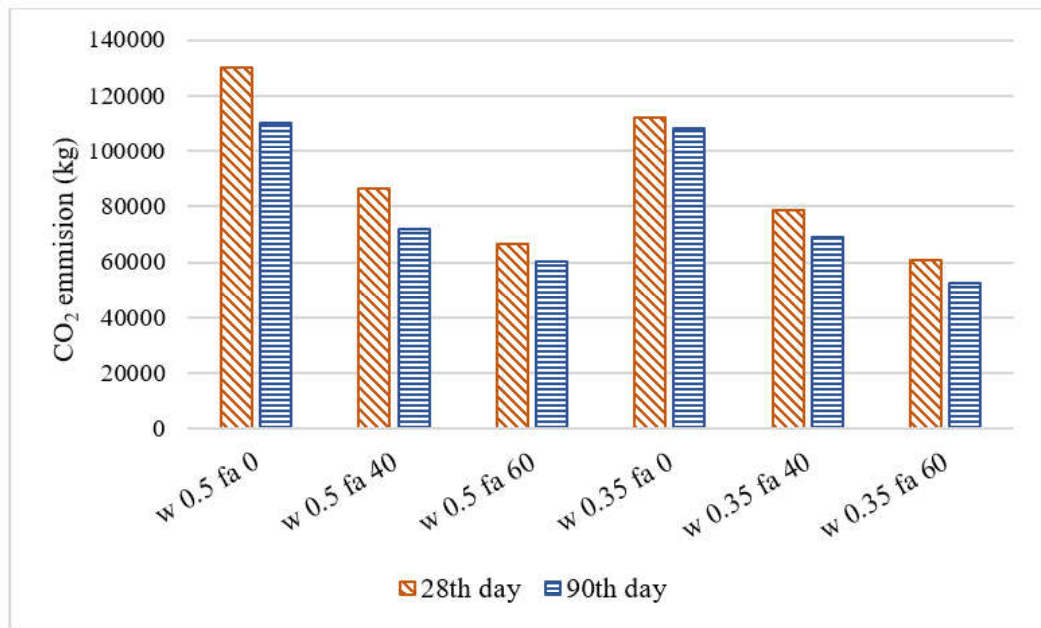


Figure 3.17. CO₂ emissions for 2000 m² industrial floor with design thickness.

It can be clearly seen from Figure 3.17 that the CO₂ emissions were decreasing with an increase in fly ash replacement level despite the increase in the required thickness. This decrease is caused by the enormous difference in the CO₂ equivalent values which is a standard unit for measuring carbon footprints, between cement and fly ash (Table 2.11). It was also decreasing with the decrease in the W/B ratio, due to the decrease in the required thickness with increment in strength.

3.4.3. Economic Analysis for 2000 m² Industrial Floor

While calculating the cost of the 2000 m² slabs, prices taken from a local trader were used for each ingredient of material (Table 2.12). Also, current allowance prices for CO₂ equivalents were taken into account according to the “EU Emissions Trading System (EU ETS)” report.

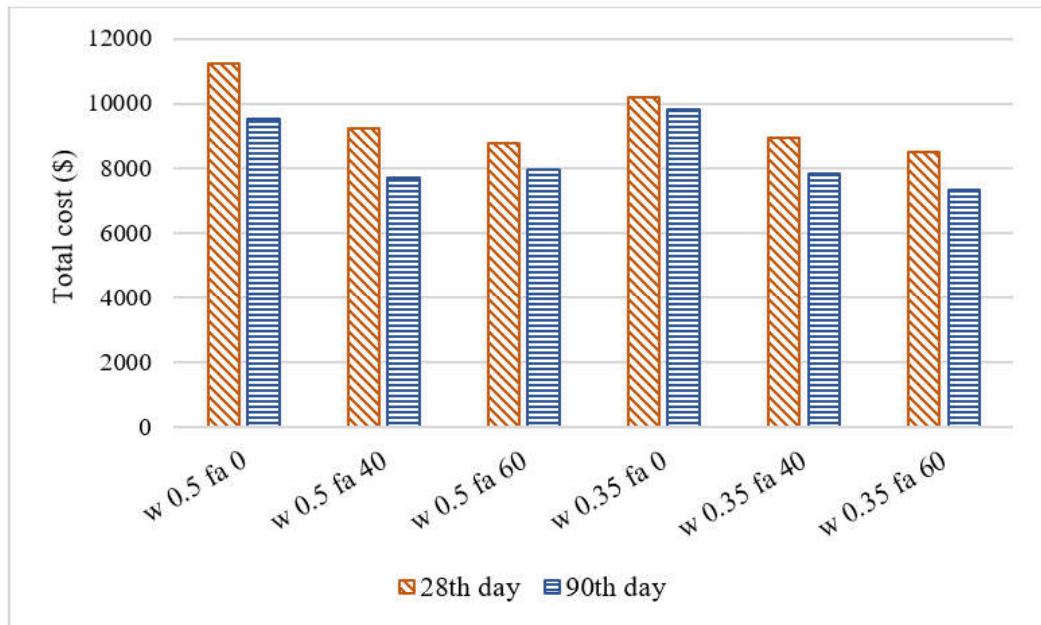


Figure 3.18. Cost for 2000 m² industrial floor with design thickness.

When Figure 3.16 and Figure 3.18 were examined together, it can be seen that despite the increase in required thickness, replacement of cement with fly ash in high amounts yields a considerable reduction in cost, and amount of decrease in cost increases with an increasing amount of replacement. However, for the “w 0.5 fa 60” mixture this statement was not valid, the cost of this mixture was very similar to the “w 0.5 fa 40” mixture at the age of 90 days. Since the strength of this mixture is very low, the required thickness was found very high even when 90 day strength value was considered. However, it can be said that costs were decreased with an increase in fly ash replacement level, except low strength concrete mixture. Also decreasing the W/B ratio causes a decrease in cost since a thinner slab is required for higher strength material.

4. CONCLUSION

This study was conducted in order to understand fresh state behavior, strength properties and, durability behaviors of high-volume fly ash concrete. After that, the effect of fly ash replacement by means of cost and CO₂ emission was examined for the same load condition.

- An increase in fly ash replacement level resulted in an increment in the slump. This can be interpreted as higher workability. Since all mixtures were aimed to be produced in the same workability class, mixtures with higher fly ash required less superplasticizer. This situation concluded less cost than other mixtures.
- Compressive and flexural strength of specimens were decreased with increasing replacement levels of fly ash. However, this decrement can be compensated with a reduction in the W/B ratio.
- There is a strong relationship between flexural strength and both initial cracking toughness and unstable fracture toughness. Similarly, these were also decreased with increment in fly ash replacement ratio, and this decrement can be compensated with W/B ratio adaptation.
- The dynamic modulus of elasticity results showed that the elastic modulus of concrete did not change with age. An increase in fly ash percentage caused a decrease in elastic modulus parallel to compressive strength. However, the effect of the W/B ratio change was slightly more than the effect of fly ash amount change. So, the decreasing elastic modulus effect of the fly ash replacement ratio can be eliminated by a small decrease in the W/B ratio.
- From water absorption test results, it was seen that fly ash increment concluded concrete with a more permeable void. This situation caused a discontinuity in concrete and led to a decrease in strength.
- There was no meaningful relationship between the rate of absorption and fly ash replacement. However, the initial rate of absorptions was increased for all mixtures and the secondary rate of absorptions was decreased for the mixtures

with fly ash.

- Fly ash replacement ratio or W/B ratio differences did not affect length change remarkably. All specimens get shorter in the first days, then their length change became slower and stopped.
- The damage created by abrasion on specimens had a reverse relation with flexural strength. Fly ash replacement caused a decrease in flexural strength and an increase in abrasion damage. It can be concluded that abrasion resistance was also increased with an increment in flexural strength.
- No constant relationship was observed between fly ash replacement level and freeze-thaw durability. None of the specimens with a higher W/B ratio could achieve a 300 freeze thaw cycle. The best performance was achieved with the concrete with a low W/B ratio and the highest fly ash replacement level in this study.
- An increase in fly ash level led to an increase in thickness for the industrial floor since it caused a decrease in flexural strength. However, an increment in thickness does not necessarily mean an increment in cost. While increment of fly ash level decreased total CO₂ emission due to lower CO₂ equivalent of fly ash than cement, this study also showed that it also led to decrease in cost.

The main purpose of this study was to examine the effect of high amount cement reduction in concrete by replacing it with fly ash. This study showed that high volume fly ash concrete at a low W/B ratio is an alternative to conventional Portland cement concrete. The outputs of this study showed not only HVFAC is an alternative for PCC but also it is more economic and more environmentally friendly.

REFERENCES

1. Zhang, J., G. Liu, B. Chen, D. Song, J. Qi, and X. Liu, "Analysis of CO₂ Emission for the Cement Manufacturing with Alternative Raw Materials: A Life Cycle Assessment Based Framework", *Energy Procedia*, Vol. 61, pp. 2541-2545, 2014.
2. Andrew, R. M., "Global CO₂ Emissions From Cement Production", *Earth System Science Data*, Vol. 10, No. 1, pp. 195-217, 2018.
3. Matos, P., M. Foiato, and L. R. Jr, "Ecological, Fresh State and Long-Term Mechanical Properties of High-Volume Fly Ash High-Performance Self-Compacting Concrete", *Construction and Building Materials*, Vol. 203, pp. 282-293, 2019.
4. Lam, L., Y. Wong, and C. S. Poon, "Degree of Hydration and gel/Space Ratio of High-Volume fly ash/Cement Systems", *Cement and Concrete*, Vol. 30, pp. 747-756, May 2000.
5. Yu, J., C. Lu, C. K. Y. Leung, and G. Li, "Mechanical Properties Of Green Structural Concrete With Ultrahigh-Volume Fly Ash", *Construction and Building Materials*, Vol. 147, pp. 510-518, 2017.
6. Heidrich, C., H. Feuerborn, and A. Weir, "Coal Combustion Products: a Global Perspective", *Stay Connected With Semantic Scholar*, Vol. 45, No. 45021704, 2013.
7. Tokyay, M., *Cement and Concrete Mineral Admixtures*, Routledge; Reprint, 2016.
8. Berg W. and H. Feuerborn, "25 Present Situation and Perspectives of CCP Management in Europe", *International Energy Agency's Clean Coal Centre*, No. 15, pp. 1-10, 2005.
9. Das, S., R. Kohnlechner, F. Aman, and L. Dascalescu, "Corona Separation of Fly Ash", *2007 IEEE Industry Applications Society Annual Meeting*, pp. 792-799, 2007.

10. Wesche, K., *Fly Ash in Concrete: Properties and Performance. Report of Technical Committee 67-FAB Use of fly ash in Buildings*, London: Spon, 1991.
11. Wesche, K. *Fly Ash in Concrete: Properties and Performance*, Taylor and Francis, 2004.
12. Swamy, R.N., *Cement Replacement Materials*, Surrey University Press, 1986.
13. American Society for Testing and Materials ASTM, "Standard Specification for Coal Fly Ash and Raw or Calcined Natural Pozzolan for Use", *Annual Report, Board of Directors Information American Society for Testing and Materials Stand*, No. C, pp. 3-6, 2019.
14. British Standards Institution, *BS EN 197-1:2011 British Standards Institution BSI Standards Publication Cement*, 2011.
15. Mohanraj, K., G. Sivakumar, and S. Barathan, "Hydration Process of Fly Ash Blended Cement Composite", *International Journal of Chemical Sciences*, Vol. 8, No. 1, pp. 589-601, 2010.
16. British Standards Institution, "BSEN 206:2013: BSI Standards Publication Concrete - Specification, Performance", *Production and Conformity, Bayerischer Rundfunk Stands*, 2013.
17. Du, S., Y. Jiang, J. Zhong, Y. Ge, and X. Shi, "Surface Abrasion Resistance of High-Volume Fly Ash Concrete Modified by Graphene Oxide: Macro- and Micro-Perspectives", *Construction and Building Materials*, Vol. 237, pp. 117686, 2020.
18. Zhao, Z., K. Wang, D.A. Lange, H. Zhou, W. Wang, and D. Zhu, "Creep and Thermal Cracking of Ultra-High Volume Fly Ash Mass Concrete at Early Age", *Cement and Concrete Composites*, Vol. 99, pp. 191-202, 2019.
19. Helmuth, R., *Fly Ash in Cement and Concrete*, Skokie, Ill: Portland Cement

Assoc., 1987.

20. Raymond, R.W.C., E. Davis J.W. Kelly, Harmer E. Davis, “Properties of Cements and Concretes Containing Fly Ash”, *Airports Council International ACI Journal Process*, Vol. 33, No. 5, 2008.
21. de Matos, P.R., M. Foiato, and L.R. Prudencio, “Ecological, Fresh State and Long-Term Mechanical Properties of High-Volume Fly Ash High-Performance Self-Compacting Concrete”, *Construction and Building Materials*, Vol. 203, pp. 282-293, 2019.
22. Huang, Q., X. Zhu, D. Liu, L. Zhao, and M. Zhao, “Modification of Water Absorption and Pore Structure of High-Volume Fly Ash Cement Pastes By Incorporating Nanosilica”, *Journal of Building Engineering*, Vol. 33, No. March 2020, pp. 101638, 2021.
23. Jiang, P., L. Jiang, J. Zha, and Z. Song, “Influence of Temperature History on Chloride Diffusion in High Volume Fly Ash Concrete”, *Construction and Building Materials*, Vol. 144, pp. 677-685, 2017.
24. Karahan, O., “Transport Properties of High Volume Fly Ash or Slag Concrete Exposed to High Temperature”, *Construction and Building Materials*, Vol. 152, pp. 898-906, 2017.
25. Lam, L., Y.L. Wong, and C.S. Poon, “Degree of Hydration and Gel/Space Ratio of High-Volume Fly Ash/Cement Systems”, *Cement and Concrete*, Vol. 30, No. 5, pp. 747-756, 2000.
26. Sherir, M.A.A., K.M.A. Hossain, and M. Lachemi, “Fresh State, Mechanical and Durability Properties of Strain Hardening Cementitious Composite Produced with Locally Available Aggregates and High Volume of Fly Ash”, *Construction and Building Materials*, Vol. 189, pp. 253-264, 2018.


27. Ammasi A.K., and Ragul, “Strength and Durability of High Volume Fly Ash in Engineered Cementitious Composites”, *Materials Today: Proceedings*, Vol. 5, No. 11, pp. 24050-24058, 2018.
28. Golewski, G.L., “Generalized Fracture Toughness and Compressive Strength of Sustainable Concrete Including Low Calcium Fly Ash”, *Materials (Basel)*, Vol. 10, No. 12, 2017.
29. Mardani-Aghabaglou, A., Ö. Andiç-Çakir, and K. Ramyar, “Freeze-Thaw Resistance and Transport Properties of High-Volume Fly Ash Roller Compacted Concrete Designed by Maximum Density Method”, *Cement and Concrete Composites*, Vol. 37, No. 1, pp. 259-266, 2013.
30. British Standard Institute *BSI Standards Publication Method of Testing Cement Part 2: Chemical Analysis of Cement*, British Standards Online, 2013.
31. British Standard Institute BS EN 196-3:, *Methods of Testing Cement - Part 3: Determination of Setting Times and Soundness*, Bayerischer Rundfunk BR Series, STAND, 2016.
32. British Standards Institution *BSI, BS EN 196-6:2018 Methods of Testing Cement, Part 6: Determination of Fineness*, British Standards Online, 2018.
33. Business Software Alliance BSA, “British Standards Institution BSI Standards Publication Methods of testing cement Part 1: Determination of strength”, *British Standards Bs En 196-12016*, pp. 1-33, 2016.
34. British Standards Institution BSI, *BSI Standards Publication Fly ash for concrete Part 1: Definition, Specifications and Conformity Criteria*, British Standards Online, 2012.
35. British Standards Institution BSI, *BSI Standards Publication Method of Testing Fly Ash*, British Standards Online, 2017.

36. British Standards Institution BSI, *BSI Standards Publication Tests for Mechanical and Physical Properties of Aggregates Part 6: Determination of Particle Density and Water Absorption*, British Standards Online, 2013.
37. European Committee for Standardization, “BSI Standards Publication Tests for Geometrical Properties of Aggregates Part 1: Determination of Particle Size Distribution - Sieving Method”, *Bayerischer Rundfunk Br Standard Institution*, Vol. 933, 2012.
38. Turkish Standards Institution TSI, *TS 802 Design of Concrete Mixes*, No. 112, 2019.
39. British Standards Institution BSI, “BSEN 12350-8:2019, BSI Standards Publication Testing Hardened Concrete”, *Br Standard*, pp. 18, 2019.
40. British Standards Institution BSI “British Railways Standard Publication Testing Fresh Concrete”, *British Railways Standard*, 2019.
41. Japanese Concrete Institute, “Method of Test for Fracture Energy of Concrete by Use of Notched Beam”, *Japan Concrete Institute Standard*, Vol. 2, No. 2, pp. 1-14, 2003.
42. Chen, G.M., H. Yang, C.J. Lin, J.F. Chen, Y.H. He, and H.Z. Zhang, “Fracture Behaviour of Steel Fibre Reinforced Recycled Aggregate Concrete After Exposure to Elevated Temperatures”, *Construction and Building Materials*, Vol. 128, pp. 272-286, 2016.
43. Akturk, B., A.H. Akca, and A.B. Kizilkanat, “Fracture Response of Fiber-Reinforced Sodium Carbonate Activated Slag Mortars”, *Construction and Building Materials*, Vol. 241, pp. 118128, 2020.
44. Xu, S., and H.W. Reinhardt, “Determination of Double-K Criterion for Crack Propagation in Quasi-Brittle Fracture, Part I: Experimental Investigation of Crack

- Propagation”, *International Journal of Fracture*, Vol. 98, No. 2, pp. 111-149, 1999.
45. Kumar, S., and S.V. Barai, “Determining the Double-K Fracture Parameters for Three-Point Bending Notched Concrete Beams Using Weight Function”, *Fatigue and Fracture of Engineering Materials and Structures*, Vol. 33, No. 10, pp. 645-660, 2010.
 46. American Society for Testing and Materials ASTM Standard C215, “Standard Test Method for Fundamental Transverse , Longitudinal and Torsional Resonant Frequencies of Concrete Specimens”, *American Society for Testing and Materials ASTM Standard*, pp. 1-7, 2008.
 47. American Society for Testing and Materials ASTM C642, “Standard Test Method for Density, Absorption, and Voids in Hardened Concrete, ASTM International, United States”, *Annual Book of ASTM Standards*, pp. 1-3, 2013.
 48. American Society for Testing and Materials ASTM C1585-13, “Standard Test Method for Measurement of Rate of Absorption of Water by Hydraulic Cement Concretes”, *American Society for Testing and Materials ASTM International*, Vol. 41, No. 147, pp. 1-6, 2013.
 49. American Society for Testing and Materials ASTM C1202, “Standard Test Method for Electrical Indication of Concrete’s Ability to Resist Chloride Ion Penetration”, *American Society for Testing and Materials ASTM*, No. C, pp. 1-8, 2012.
 50. American Society for Testing and Materials ASTM:C157/C157M-08, “Standard Test Method for Length Change of Hardened Hydraulic-Cement Mortar and Concrete”, *American Society for Testing and Materials ASTM International*, Vol. 08, pp. 1-7, 2008.
 51. American Society for Testing and Materials ASTM C490/C490M, “Standard practice for use of apparatus for the determination of length change of hardened cement

- paste, mortar and Concrete Society 490”, *Annual Reports Section “B” of ASTM American Society for Testing and Materials*, No. C, pp. 1-5, 2007.
52. American Society For Testing And Materials, ASTM C1747, “Standard Test Method for Determining Potential Resistance to Degradation of Pervious Concrete by Impact and Abrasion”, *American Society For Testing And Materials, ASTM C1747/C1747M-13*, pp. 2-5, 2013.
 53. American Society For Testing and Materials ASTM C666/C666M, “Standard Test Method for Resistance of Concrete to Rapid Freezing and Thawing”, *ASTM Int. West Conshohocken*, Vol. 03, pp. 1-6, 2003.
 54. Concrete Society, *TR 34 Concrete Industrial Ground Floors Fourth Edition*, Vol. 29, No. 1, 2016.
 55. Turkish Standards Institution T.S. Institue, *TS 500 Requirements for Design and Construction of Reinforced Concrete Structures*, 2000.
 56. Geoff Hammond, C.J., *Inventory of Carbon and Energy (Ice)*, 2008.
 57. Mulvaney, D., “Green New Deal”, *Solar Power*, pp. 47-65, 2019.
 58. Rao, S.K., P. Sravana, and T.C. Rao, “Abrasion Resistance and Mechanical Properties of Roller Compacted Concrete with GGBS”, *Construction and Building Materials*, Vol. 114, pp. 925-933, 2016.
 59. Concrete Society, “TR 34 Concrete Industrial Ground Floors Third Edition”, 2003.

APPENDIX A: COPYRIGHTS OF FIGURES



Corona Separation of Fly Ash

Author: Subhankar Das
 Publication: IEEE Transactions on Industry Applications
 Publisher: IEEE
 Date: Nov.-Dec. 2010

Copyright © 2010, IEEE

Thesis / Dissertation Reuse

The IEEE does not require individuals working on a thesis to obtain a formal reuse license, however, you may print out this statement to be used as a permission grant:

Requirements to be followed when using any portion (e.g., figure, graph, table, or textual material) of an IEEE copyrighted paper in a thesis:

- 1) In the case of textual material (e.g., using short quotes or referring to the work within these papers) users must give full credit to the original source (author, paper, publication) followed by the IEEE copyright line © 2011 IEEE.
- 2) In the case of illustrations or tabular material, we require that the copyright line © [Year of original publication] IEEE appear prominently with each reprinted figure and/or table.
- 3) If a substantial portion of the original paper is to be used, and if you are not the senior author, also obtain the senior author's approval.

Requirements to be followed when using an entire IEEE copyrighted paper in a thesis:

- 1) The following IEEE copyright/ credit notice should be placed prominently in the references: © [year of original publication] IEEE. Reprinted, with permission, from [author names, paper title, IEEE publication title, and month/year of publication]
- 2) Only the accepted version of an IEEE copyrighted paper can be used when posting the paper or your thesis on-line.
- 3) In placing the thesis on the author's university website, please display the following message in a prominent place on the website: In reference to IEEE copyrighted material which is used with permission in this thesis, the IEEE does not endorse any of [university/educational entity's name goes here]'s products or services. Internal or personal use of this material is permitted. If interested in reprinting/republishing IEEE copyrighted material for advertising or promotional purposes or for creating new collective works for resale or redistribution, please go to http://www.ieee.org/publications_standards/publications/rights/rights_link.html to learn how to obtain a License from RightsLink.

If applicable, University Microfilms and/or ProQuest Library, or the Archives of Canada may supply single copies of the dissertation.

BACK
CLOSE WINDOW

Figure A.1. Copyrights of Figure 1.1.